ENHANCEMENT OF FREE SPECTRAL RANGE FREQUENCY USING RING RESONATORS

CHAIWAT SIRAWATTANANON

A THESIS SUBMITTED IN PARTIAL FULFILLMENT

OF THE REQUIREMENT FOR THE DEGREE OF

MASTER OF ENGINEERING IN COMPUTER ENGINEERING

FACULTY OF ENGINEERING

KING MONGKUT'S INSTITUTE OF TECHNOLOGY LADKRABANG

2011

KMITL-2011-EN-M-070-076

หัวข้อวิทยานิพนธ์	การปรับปรุงแถบสเปกตรัมเชิงความถี่โดยใช้โพรงสั่นพ้องแบบวงแหวน
นักศึกษา	นายชัยวัฒน์ ศิระวัฒนานนท์
รหัสประจำตัว	52611007
ปริญญา	วิศวกรรมศาสตรมหาบัณฑิต
สาขาวิชา	วิศวกรรมคอมพิวเตอร์
พ.ศ.	2554
อาจารย์ที่ปรึกษาวิทยานิพนธ์	รศ.ดร.สมศักดิ์ มิตะถา

บทคัดย่อ

วิทยานิพนธ์นี้นำเสนอผลวิจัยที่ได้จากอุปกรณ์ชนิดไม่เป็นเชิงเส้น โดยใช้โพรงสั่นพ้องแบบวงแหวนขนาดเล็ก เพื่อใช้ในการประมวลผลสัญญาณทางแสงซึ่งสามารถประยุกต์ใช้กับระบบการสื่อสารทางแสงและการส่งข้อมูลที่ต้องการรักษาความปลอดภัยของข้อมูลได้

การเพิ่มประสิทธิภาพด้วยวิธีมัลติเพล็กซ์แบบแบ่งความยาวคลื่นDWDMนั้นทำให้ช่องสัญญาณมีความจุที่เพิ่มมากขึ้นและสัญญาณมีความปลอดภัยสูง การเพิ่มจำนวนของช่องสัญญาณสามารถทำได้โดยทำให้ความยาวคลื่นมีความหนาแน่นเพิ่มขึ้น ขณะที่ความปลอดภัยของข้อมูลเกิดจากการเลือกใช้ความยาวคลื่นที่เฉพาะเจาะจง ดังผลงานวิจัยที่ได้แสดงถึงการเพิ่มช่องสัญญาณที่นำไปใช้ได้ในการสื่อสารทางแสงซึ่งข้อดีคือ ระบบที่ได้นำเสนอนั้นสามารถสร้างและใช้งานได้จริงร่วมกับระบบสื่อสารที่มีอยู่ เพื่อตอบสนองต่อความต้องการที่ไม่มีขีดจำกัดทางแบนด์วิดท์และการเชื่อมต่อต่างๆในยุคสมัยนี้

ระบบที่ได้นำเสนอในงานวิจัยนี้ประกอบด้วย โพรงสั่นพ้องแบบวงแหวนขนาดเล็กประกอบกับตัวกรองสัญญาณ add/drop ในกระบวนการเริ่มจากการป้อนพัลส์แบบเกาส์เซียนเข้าไปในอุปกรณ์ชนิดไม่เป็นเชิงเส้นจะได้สเปกตรัมของแสงที่มีความต่อเนื่อง ซึ่งสามารถนำมาใช้งานได้โดยการเลือกช่วงของสัญญาณที่ต้องการจากสัญญาณเอาท์พุตความถี่สูงที่สร้างได้

Thesis	Enhancement of Free Spectral Range Frequency Using Ring Resonators
Student	Mr.Chaiwat Sirawattananon
Student ID.	52611007
Degree	Master of Engineering
Program	Computer Engineering
Year	2011
Thesis Advisor	Assoc.Prof.Dr.Somsak Mitatha

ABSTRACT

This thesis presents a results of the nonlinear device known as a nonlinear micro ring resonator to process the optical signal processing which can be applied to the optical communication systems and secured data transmission.

We propose the dense wavelength division multiplexing (DWDM) wavelength enhancement, whereas the increasing in channel capacity and signal security can be provided. The increasing in number of channel can be obtained by the increasing in wavelength density, while the security is introduced by the specific wavelength filter. The optical communication wavelength enhancement is reviewed. The advantage is that the proposed system can be implemented and used incorporating with the existed communication system to satisfy these never-ending demands for bandwidth and connectivity in sophisticated.

A system consists of a micro ring resonator system incorporating an add/drop filter. In operation, a Gaussian pulse is input into a nonlinear device system and the continuous spectrum of light can be generated. In application, the selected of the required optical output for high frequency signal can be generated and achieved.

CONTENTS

CONTENTS (Cont.)

LIST OF FIGURES

Figures Pages

LIST OF FIGURES (Cont.)

LIST OF TABLES

CHAPTER 1

INTRODUCTION

1.1 Optical Communication System

[1] Optical systems represent a natural extension of microwave communication systems inasmuch as information is transmitted over an electromagnetic carrier in both types of systems. The major difference from a conceptual standpoint is that, whereas carrier frequency is typically ~ 1 GHz for microwave systems, it increases by five orders of magnitude and is typically ~ 100 THz in the case of optical systems. This increase in carrier frequency translates into a corresponding increase in the system capacity. Indeed, whereas microwave systems rarely operate above 0.2 Gb/s, commercial optical systems can operate at bit rates exceeding 1 Tb/s. Although the optical carrier is transmitted in free space for some applications related to satellites and space research, terrestrial optical systems often employ optical fibers for information transmission. Such fiber-optic communication systems have been deployed worldwide since 1980 and constitute the backbone behind the Internet. At the dawn of the twenty-first century, the emphasis of optic communication systems was on increasing the system capacity by transmitting more and more channels through the WDM technique with increasing WDM signal bandwidth. To enhance the spectral efficiency by adopting new modulation formats, while increasing the bit rate of each WDM channel. Such systems require an extremely careful management of fiber dispersion. Novel techniques capable of compensating chromatic and polarization-mode dispersions in a dynamic fashion are being developed to meet such challenges. An interesting approach is based on the concept of optical solitons-pulses that preserve their shape during propagation in a lossless fiber by counteracting the effect of dispersion through the fiber nonlinearity. As mentioned earlier, optical systems differ from microwave systems only in the frequency range of the carrier wave used to carry the information. Both types of systems can be divided into three major parts. Figure 1.1 shows a generic optical communication system consisting of an optical transmitter, a communication channel, and an optical receiver. Optical systems can be classified into two broad categories depending on the nature of the communication channel. The optical signal propagates unguided in air or vacuum for some applications. However, in the case of guided optical systems, the optical beam emitted by the transmitter remains spatially confined inside an optical fiber.

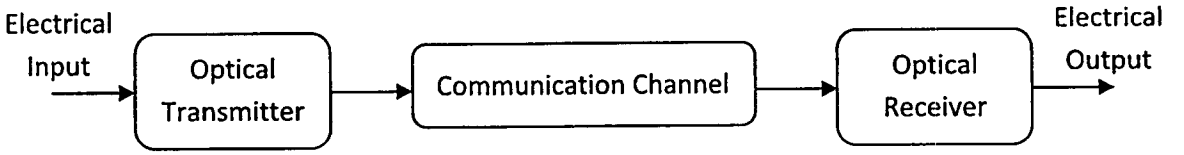

Figure 1.1 A generic optical communication system.

1.2 Optical Transmission System

[2] Optical transmission links have been built all around the globe. High-capacity submarine optical transmission links are being built to connect continents and provide protected transmission of data, while multiple terrestrial physical optical fiber-based networks have been built both for transmission and distribution of different bandwidth channels. The optical fiber connection has been coming all the way down to the curb, building, home, and the desk.

The ultimate goal of proper optical system engineering is to deliver the information bandwidth from one physical location to the other in the most economical way, while achieving required QoS. This can be done by establishing the most favorable relationship between a number of variables that characterize the signal and different impairments (such as noise, nonlinear effects) within a specific transmission scenario. The scope of the optical transmission system engineering is to understand how to minimize the effect of different impairments, learn how to allocate system margin to cape with remaining destructive effects, and how to make trade-offs between different design parameters to achieve the goal mentioned above.

The simplest optical transmission system is a point-to-point connection that utilizes a single optical wavelength, which propagates through an optical fiber. The upgrade to this topology is deployment of the wavelength division multiplex (WDM) technology, where multiple optical wavelengths are combined to travel over the same physical route.

The WDM has proven to be a cost-effective means of increasing the bandwidth of installed fiber plant. While the technology originally only served to increase the size of the fiber spans, it gradually became the foundation for optical networks. In an optical networking scenario, different signals are transported over arbitrary distances, while the wavelength routing can take a place at specified locations. The WDM technology is sometimes named with different prefixes—

dense-WDM (DWDM), course-WDM (CWDM), or ultra-dense-WDM (UDWDM)—used to reflect a specific multiplexing technique used.

Several optical channels, associated with specified information bandwidth, have been combined by WDM technology and sent to the optical fiber line. The aggregated signal is then transported over some distance before it is demultiplexed and converted back to an electrical level by a photodetection process. The optical signal transmission path can include a number of optical amplifiers, optical cross-connects, and optical add-drop multiplexers. The optical signal on its way from the source to the destination can be processed by various optical components, such as optical filters, optical attenuators, and optical isolators.

There are several types of optical transmission systems. If using the transmission length as a criterion, all systems can be classified as (1) very short reach (VSR) with lengths measured in hundreds of meters, (2) short reach (SR) with lengths measured in kilometers, (3) long reach (LR) with lengths measured in tens and hundreds of kilometers, and (4) ultra-long reach (ULR) with lengths measured in thousands of kilometers. If using the bit rate as a criterion, optical transmission systems can be (1) low-speed with bit rates measured in tens of megabits per second, (2) medium-speed with bit rates measured in hundreds of megabits per second, and (3) high-speed with bit rates measured in gigabits per second. Finally, from the application perspective, transmission systems are either power budget limited (or loss limited), or transmission speed (or bandwidth) limited.

The ultimate goal of optical signal transmission is usually defined as achieving the specified bit error rate (BER) between two end users, or between two separate intermediate points. Optical transmission system needs to be properly engineered in order to provide stable and reliable operation during its lifetime, which includes the management (setup, fine tuning, trade-offs) of key engineering parameters.

1.3 Goal of the Thesis

For the full utilization of large bandwidth and high speed features provided by optical fibers, currently concepts for integrated optical devices for wavelength division multiplexing/demultiplexing are vigorously investigated. Due to their superior selectivity, compactness, optical performances, flexibility and possibility of dense integration, micro resonators with circular ring are attractive add-drop filter elements for applications in photonic chips related to optical wavelength division multiplexing. Micro ring resonators with these requirements are thus need careful and exact design for their correct operation. A direct result of the progress in fabrication techniques is the increased need of the accurate models for characterizing the filters. For very simple devices, analytical tools provide a framework for quick low cost feasibility studies and allow for design optimization before devices are fabricated.

The primary goal of this thesis investigates the design and simulation nonlinear characteristics of ring resonator architectures. The discrete-time signal processing (DSP) approach is systematic and intuitive for the design of nonlinear optical devices and also found that very useful for fast deriving an algorithm transfer functions in Z-domain for modeling ring resonator and add/drop filter. Those devices can be enhancement of free spectral range frequency.

1.4 Scope of the Thesis

With the growing importance of micro ring resonators for a variety of applications, it becomes necessary to devise a model which is directly interpretable in physical terms, and which is essentially free of any fit parameters. In this thesis, we restrict ourselves to the design of 2-D a multiple ring resonator filters and analyze the nonlinear characteristics in general. In this thesis, we employ the discrete-time signal processing (DSP) approach to design and analyze nonlinear optical filters. DSP is employed here for the analytical derivation of the optical transfer functions in Z-domain of filters. The present analysis is restricted to directional couplers and waveguides characterized by various parameters, the power coupling coefficient, power coupling loss, the radius of the ring waveguide and attenuation coefficient.

1.5 Organization of the Thesis

This thesis presents a design and simulated characteristics for characterizing nonlinear optical ring resonator filters. The organization is as follows:

- The current chapter gives an introduction to the subject of the thesis.
- Chapter 2 describes propagation of signals in optical fiber and some of phenomena of nonlinear optic.
- Chapter 3 describes ring resonator characterization, analytical derivation of the optical transfer functions in Z-domain and enhanced nonlinearity in ring resonator.
- Chapter 4 proposes a system of frequency divider design using micro ring resonator that can be generated and enhanced multi frequency bands.
- Finally, Chapter 5 presents a summary of the results of the thesis and a discussion of future research.

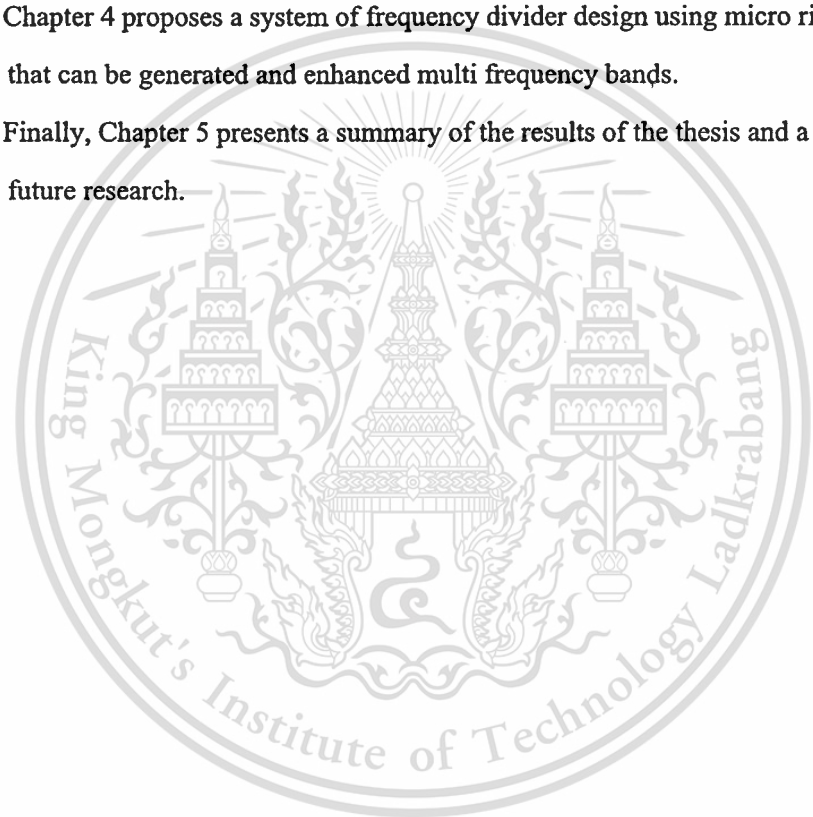

CHAPTER 2

THEORETICAL BACKGROUND

2.1 Waveguide Structure

Optical fibers and optical waveguides consist of a core, in which light is confined, and a cladding, or substrate surrounding the core, as shown in Fig. 2.1. The refractive index of the core n_1 is higher than that of the cladding n_0. Therefore the light beam that is coupled to the end face of the waveguide is confined in the core by total internal reflection. The condition for total internal reflection at the core–cladding interface is given by $n_1 \sin(\pi/2 - \emptyset) \geq n_0$. Since the angle $\emptyset$ is related with the incident angle θ by $\sin\theta = n_1 \sin\emptyset \leq \sqrt{n_1^2 - n_0^2}$, we obtain the critical condition for the total internal reflection as

$$\theta \leq \sin^{-1}\sqrt{n_1^2 - n_0^2} \equiv \theta_{max} \tag{2.1}$$

The refractive-index difference between core and cladding is of the order of $n_1 - n_0 = 0.01$. Then θ_{max} in Eq. (2.1) can be approximated by

$$\theta_{max} \cong \sqrt{n_1^2 - n_0^2} \tag{2.2}$$

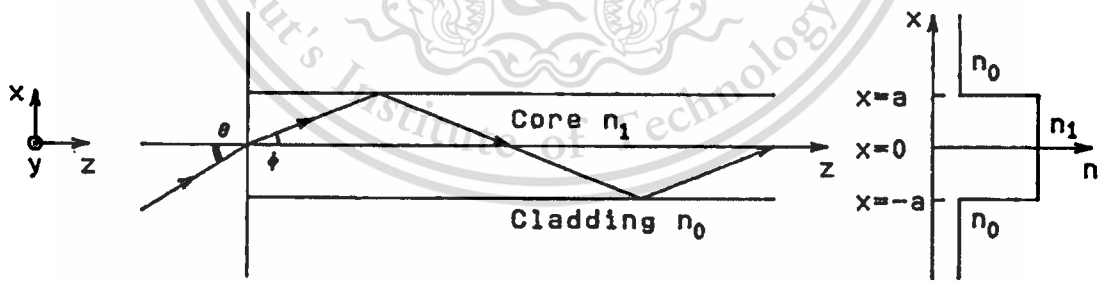

Figure 2.1 Basic structure and refractive-index profile of the optical waveguide.

θ_{max} denotes the maximum light acceptance angle of the waveguide and is known as the numerical aperture (NA).

The relative refractive-index difference between n1 and n0 is defined as

$$\Delta = \frac{n_1^2 - n_0^2}{2n_1^2} \cong \frac{n_1 - n_0}{n_1} \tag{2.3}$$

Δ is commonly expressed as a percentage. The numerical aperture NA is related to the relative refractive-index difference Δ by

$$NA = \theta_{max} \cong n_1\sqrt{2\Delta} \tag{2.4}$$

The maximum angle for the propagating light within the core is given by $\emptyset_{max} \cong \theta_{max}/n_1 \cong \sqrt{2\Delta}$. For typical optical waveguides, NA = 0.21 and $\theta_{max} = 12°(\emptyset_{max} = 8.1°)$ when n_1 = 1.47 , Δ = 1% (for n_0=1.455).

2.2 Nonlinear Optics

Nonlinear optics is the area of optics that studies the interaction of light with matter in the regime where the response of the material system to the applied electromagnetic field is nonlinear in the amplitude of this field. At low light intensities, typical of non-laser sources, the properties of materials remain independent of the intensity of illumination. The superposition principle holds true in this regime, and light waves can pass through materials or be reflected from boundaries and interfaces without interacting with each other. Laser sources, on the other hand, can provide sufficiently high light intensities to modify the optical properties of materials. Light waves can then interact with each other, exchanging momentum and energy, and the superposition principle is no longer valid. This interaction of light waves can result in the generation of optical fields at new frequencies, including optical harmonics of incident radiation or sum- or difference-frequency signals.

Although the observation of most nonlinear-optical phenomena requires laser radiation, some classes of nonlinear-optical effects were known long before the invention of the laser. The most prominent examples of such phenomena include Pockels and Kerr electrooptic effects [26], as well as light-induced resonant absorption saturation, described by Vavilov [27, 28]. It was, however, only with the advent of lasers that systematic studies of optical nonlinearities and the observation of a vast catalog of spectacular nonlinear-optical phenomena became possible.

In the first nonlinear-optical experiment of the laser era, performed by Franken et al. in 1961 [29], a rubylaser radiation with a wavelength of 694.2 nm was used to generate the second harmonic in a quartz crystal at the wavelength of 347.1 nm. This seminal work was followed by the discovery of a rich diversity of nonlinear-optical effects, including sum-frequency generation, stimulated Raman scattering, self-focusing, optical rectification, four-wavemixing, andmany

others. While in the pioneering work by Franken the efficiency of second-harmonic generation (SHG) was on the order of 10^{-8}, optical frequency doublers created by early 1963 provided 20% - 30% efficiency of frequency conversion [30, 31]. The early phases of the development and the basic principles of nonlinear optics have been reviewed in the most illuminating way in the classical books by Bloembergen [32] and Akhmanov and Khokhlov [33], published in the mid 1960s. Over the following four decades, the field of nonlinear optics has witnessed an enormous growth, leading to the observation of new physical phenomena and giving rise to novel concepts and applications.A systematic introduction into these effects along with a comprehensive overview of nonlinear-optical concepts and devices can be found in excellent textbooks by Shen [34], Boyd [26], Butcher and Cotter [35], Reintjes [36] and others. One of the most recent up-to-date reviews of the field of nonlinear optics with an in-depth discussion of the fundamental physics underlying nonlinear-optical interactions was provided by Flytzanis [37]. This chapter provides a brief introduction into the main nonlinear-optical phenomena and discusses some of the most significant recent advances in nonlinear optics, as well as novel applications of nonlinear-optical processes and devices.

2.3 Nonlinear Polarization and Nonlinear Susceptibilities

Nonlinear optical effects belong to a broader class of electromagnetic phenomena described within the general framework of macroscopic Maxwell equations. The Maxwell equations not only serve to identify and classify nonlinear phenomena in terms of the relevant nonlinear optical susceptibilities or, more generally, nonlinear terms in the induced polarization, but also govern the nonlinear-optical propagation effects. We assume the absence of extraneous charges and currents and write the set of Maxwell equations for the electric, $E(r, t)$, and magnetic, $H(r, t)$, fields in the form

$$\nabla \times E = -\frac{1}{c}\frac{\partial B}{\partial t} \tag{2.5}$$

$$\nabla \times B = \frac{1}{c}\frac{\partial D}{\partial t} \tag{2.6}$$

$$\nabla \cdot D = 0 \tag{2.7}$$

$$\nabla \cdot B = 0 \tag{2.8}$$

Here, $B = H + 4\pi M$ where M is the magnetic dipole polarization, c is the speed of light, and

$$D = E + 4\pi \int_{-\infty}^{t} J(\zeta)\, d\zeta \tag{2.9}$$

where J is the induced current density. Generally, the equation of motion for charges driven by the electromagnetic field has to be solved to define the relation between the induced current J and the electric and magnetic fields. For quantum systems, this task can be fulfilled by solving the Schrödinger equation.

Formally, the current density J can be represented as a series expansion in multipoles:

$$J = \frac{\partial}{\partial t}(P - \nabla \cdot Q) + c(\nabla \times M) \tag{2.10}$$

where P and Q are the electric dipole and electric quadrupole polarizations, respectively. In the electric dipole approximation, we keep only the first term on the right-hand side of (2.10). In view of (2.9), this gives the following relation between the D, E and P vectors:

$$D = E + 4\pi P \tag{2.11}$$

We now represent the polarization P as a sum

$$P = P_L + P_{NL} \tag{2.12}$$

where P_{L} is the part of the electric dipole polarization linear in the field amplitude and P_{NL} is the nonlinear part of this polarization.

The linear polarization governs linear-optical phenomena, i.e., it corresponds to the regime where the optical properties of a medium are independent of the field intensity. The relation between P_{L} and the electric field E is given by the standard formula of linear optics:

$$P_L = \int \chi^{(1)}(t - t')E(t')dt' \tag{2.13}$$

where $\chi^{(1)}(t)$ is the time-domain linear susceptibility tensor. Representing the field E and polarization P_{L} in the form of elementary monochromatic plane waves,

$$E = E(\omega)\exp(ikr - \omega t) + c.c. \tag{2.14}$$

and

$$P_L = P_L(\omega)\exp(ikr - \omega t) + c.c. \tag{2.15}$$

we take the Fourier transform of (2.13) to find

$$P_L(\omega) = \chi^{(1)}(\omega)E(\omega) \tag{2.16}$$

where

$$\chi^{(1)}(\omega) = \int \chi^{(1)}(t)exp(i\omega t)dt \tag{2.17}$$

In the regime of weak fields, the nonlinear part of the polarization P_{NL} can be represented as a power-series expansion in the field E:

$$\begin{aligned} P_{NL} = & \iint \chi^{(2)}(t-t_1, t-t_2) : E(t_1)E(t_2)dt_1dt_2 \\ & + \iiint \chi^{(3)}(t-t_1, t-t_2, t-t_3) \\ & \vdots E(t_1)E(t_2)E(t_3)dt_1dt_2dt_3 + \ldots \end{aligned} \tag{2.18}$$

where $\chi^{(2)}$ and $\chi^{(3)}$ are the second and third-order nonlinear susceptibilities.

Representing the electric field in the form of a sum of plane monochromatic waves

$$E = \sum_i E_i(\omega_i)\exp(ik_i r - \omega_i t) + c.c. \tag{2.19}$$

we take the Fourier transform of (2.18) to arrive at

$$P_{NL}(\omega) = P^{(2)}(\omega) + P^{(3)}(\omega) + \ldots \tag{2.20}$$

where

$$P^{(2)}(\omega) = \chi^{(2)}(\omega; \omega_i, \omega_j) : E(\omega_i)E(\omega_j) \tag{2.21}$$

$$P^{(3)}(\omega) = \chi^{(3)}(\omega; \omega_i, \omega_j, \omega_k) \vdots E(\omega_i)E(\omega_j)E(\omega_k) \tag{2.22}$$

$$\begin{aligned} \chi^{(2)}(\omega; \omega_i, \omega_j) &= \chi^{(2)}(\omega = \omega_i + \omega_j) \\ &= \iint \chi^{(2)}(t_1, t_2)\exp[i(\omega_i t_1 + \omega_j t_2)]dt_1dt_2 \end{aligned} \tag{2.23}$$

is the second-order nonlinear-optical susceptibility and

$$\begin{aligned} \chi^{(3)}(\omega; \omega_i, \omega_j, \omega_k) &= \chi^{(3)}(\omega = \omega_i + \omega_j + \omega_k) \\ &= \iint \chi^{(3)}(t_1, t_2, t_3)\exp[i(\omega_i t_1 + \omega_j t_2 + \omega_k t_3)]dt_1dt_2dt_3 \end{aligned} \tag{2.24}$$

is the third-order nonlinear-optical susceptibility.

The second-order nonlinear polarization defined by (2.21) gives rise to three-wave mixing processes, optical rectification and linear electrooptic effect. In particular, setting $\omega_i = \omega_j = \omega_0$ in (2.21) and (2.23), we arrive at $\omega = 2\omega_0$, which corresponds to second-harmonic generation, controlled by the nonlinear susceptibility $\chi^{(2)}_{SHG} = \chi^2(2\omega_0; \omega_0, \omega_0)$. In a more general case of three-wave mixing process with $\omega_i = \omega_1 \neq \omega_j = \omega_2$, the second-order polarization defined by (2.21) can describe sum-frequency generation (SFG) $\omega_{SF} = \omega_1 + \omega_2$ or difference-frequency generation (DFG) $\omega_{DF} = \omega_1 - \omega_2$, governed by the nonlinear susceptibilities $\chi^{(2)}_{SFG} = \chi^{(2)}(\omega_{SF}; \omega_1, \omega_2)$ and $\chi^{(2)}_{DFG} = \chi^{(2)}(\omega_{DF}; \omega_1, -\omega_2)$, respectively.

The third-order nonlinear polarization defined by (2.22) is responsible for four-wave mixing (FWM), stimulated Raman scattering, two-photon absorption, and Kerr-effect-related phenomena, including self phase modulation (SPM) and self-focusing. For the particular case of third-harmonic generation, we set $\omega_i = \omega_j = \omega_k = \omega_0$ in (2.22) and (2.24) to obtain $\omega = 3\omega_0$. This type of nonlinear-optical interaction, in accordance with (2.22) and (2.24), is controlled by the cubic susceptibility $\chi^{(3)}_{THG} = \chi^{(3)}(3\omega_0; \omega_0, \omega_0, \omega_0)$.

2.4 Wave Aspects of Nonlinear Optics

In the electric dipole approximation, the Maxwell equations (2.5-2.8) yield the following equation governing the propagation of light waves in a weakly nonlinear medium:

$$\nabla \times (\nabla \times E) - \frac{1}{c^2}\frac{\partial^2 E}{\partial t^2} - \frac{4\pi}{c^2}\frac{\partial^2 P_L}{\partial t^2} = \frac{4\pi}{c^2}\frac{\partial^2 P_{NL}}{\partial t^2} \tag{2.25}$$

The nonlinear polarization, appearing on the right-hand side of (2.25), plays the role of a driving source, inducing an electromagnetic wave with the same frequency ω as the nonlinear polarization wave $P_{NL}(r,t)$. Dynamics of a nonlinear wave process can be then thought as a result of the interference of induced and driving (pump)waves, controlled by the dispersion of the medium.

Assuming that the fields have the form of quasimonochromatic plane waves propagating along the z axis, we represent the field E in (2.25) by

$$E(r,t) = Re[eA(z,t)\exp(ikz - \omega t)] \tag{2.26}$$

and write the nonlinear polarization as

$$P_{NL}(r,t) = Re[e_p P_{NL}(z,t)\exp(ik_p z - \omega t)] \tag{2.27}$$

where k and $A(z,t)$ are the wave vector and the envelope of the electric field, kp and $P_{NL}(z,t)$ are the wave vector and the envelope of the polarization wave.

If the envelope $A(z,t)$ is a slowly varying function over the wavelength, $|\partial^2 A/\partial Z^2| \ll |k\partial A/\partial z|$, and $\frac{\partial^2 P_{NL}}{\partial t^2} \approx -\omega^2 P_{NL}$, (2.25) is reduced to [34]

$$\frac{\partial A}{\partial z} + \frac{1}{u}\frac{\partial A}{\partial t} = \frac{2\pi i\,\omega^2}{kc^2} P_{NL}\exp(i\Delta kz) \tag{2.28}$$

where $u = (\partial k/\partial\omega)^{-1}$ is the group velocity and $\Delta k = k_p - k$is the wave-vector mismatch.

2.5 Nonlinear Refraction (Optical Kerr Effect)

Optical nonlinearity of the third order is a universal property, found in any material regardless of its spatial symmetry. This nonlinearity is the lowestorder nonvanishing nonlinearity for a broad class of centrosymmetric materials, where all the even-order nonlinear susceptibilities are identically equal to zero for symmetry reasons. Third-order nonlinear processes include a vast variety of four-wave mixing processes, which are extensively used for frequency conversion of laser radiation and as powerful methods of nonlinear spectroscopy. Frequency-degenerate, Kerr-effect-type phenomena constitute another important class of third-order nonlinear processes. Such effects lie at the heart of optical compressors, mode-locked femtosecond lasers, and numerous photonic devices, where one laser pulse is used to switch, modulate, or gate another laser pulse.

The optical Kerr effect (i.e. nonlinear refraction index) results from the third order nonlinear susceptibility $\chi^{(3)}$, which is a fourth rank tensor. It leads to a nonlinear intensity dependent contribution to its refractive index; i.e., the refractive index of the material changes as the incident intensity on the material changes. The susceptibility tensors in isotropic material can be further simplified as $\chi^{(2)} = 0$, due to inversion symmetry; the third order nonlinear susceptibility will only have one contributing term χ_{xxxx} since the light is x-polarized and there are no means for sourcing additional polarization components.

The linear and nonlinear induced polarizations are

$$P_L = \varepsilon_0(1+\chi^{(1)})E \tag{2.29}$$

and

$$
\begin{aligned}
P_{NL} &= P^{(3)} \\
&= \varepsilon_0 \chi_{xxxx}(\omega;-\omega,\omega,\omega)E^*EE \\
&\quad + \varepsilon_0 \chi_{xxxx}(\omega;\omega,-\omega,\omega)EE^*E \\
&\quad + \varepsilon_0 \chi_{xxxx}(\omega;\omega,\omega,-\omega)EEE^* \\
&= 3\varepsilon_0 \chi_{xxxx}|E|^2 E \\
&= \frac{3}{4}\varepsilon_0 \chi_{xxxx}|E_x|^2 E
\end{aligned}
\tag{2.30}
$$

respectively. Hence,

$$P = P_L + P_{NL} = \varepsilon_0\left(1 + \chi^{(1)} + \frac{3}{4}\varepsilon_0 \chi_{xxxx}|E_x|^2\right)E$$

The total dielectric constant

$$\varepsilon_r^{tot} = \varepsilon_r + \Delta\varepsilon_r$$

where $\varepsilon_r = 1 + \chi^{(1)} = n_o^2$ and $\Delta\varepsilon = \frac{3}{4}\chi_{xxxx}|E_x|^2$ after comparing with the expression for P.

The refractive index is related to the dielectric constant as:

$$n = \sqrt{\varepsilon_r + \Delta\varepsilon_r} \approx \sqrt{\varepsilon_r} + \frac{\Delta\varepsilon_r}{2\sqrt{\varepsilon_r}} = n_0 + \frac{3\chi_{xxxx}}{8n_0}|E_x|^2 \tag{2.31}$$

The intensity dependent refractive index for a nonlinear material is given by

$$n = n_0 + n_2|E|^2 \tag{2.32}$$

Comparing Eq.(2.31) and Eq.(2.32), the nonlinear refractive index is directly determined by the third-order susceptibility as

$$n_2 = \frac{3\chi_{xxxx}}{8n_0} = \frac{3\chi^{(3)}}{8n_0} \tag{2.33}$$

which characterizes the strength of the optical nonlinearity. The intensity I of an optical wave is proportional to $|E|^2$ as $I = \frac{1}{2\eta}|E|^2$ where η is the impedance of the medium. When comparing the optical response in the same medium, $I = |E|^2$ is taken for simplification.

CHAPTER 3

RING RESONATOR CHARACTERIZATION

In this chapter, I will describe the characteristics of ring resonator and theoretical background for this thesis. To begin, section 3.1 discuss the history of ring resonator and the material system which was used for the planar waveguide. Section 3.2 discusses the basic concept of optical add/drop filter. Section 3.3 discusses the key to analyzing optical filters using Z-transforms. In the section 3.4 and 3.5 discuss enhanced nonlinearity in ring resonators.

3.1 The Ring Resonator

The ring resonator is simply a waveguide shaped into a ring structure as shown in Figure 3.1. When an input electric field, E_i is coupled to the ring waveguide through an external bus waveguide, a positive feedback is induced and the field inside the ring resonator, E_r starts to build up. Coupling between the straight and the ring waveguide is achieved through the evanescent wave. Therefore, the gap and coupling length between them determine how much power is coupled from the straight waveguide to the ring waveguide and vise versa. The feedback mechanism is simply induced by the ring waveguide and therefore there is no need for any Bragg gratings, mirrors, or distributed feedback waveguides which are more difficult to fabricate. In such configuration, only certain wavelengths will be allowed to resonate inside the ring waveguide, thus frequency selectivity is obtained.

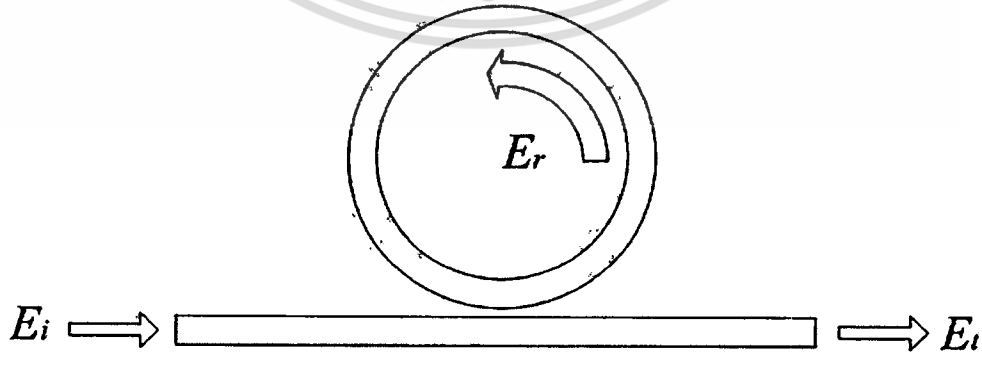

Figure 3.1 Schematic diagram for a ring resonator coupled to a single waveguide.

The proposal to use an integrated ring resonator for a bandpass filter has been made in 1969 by E. A. Marcatili [9]. The layout of the channel dropping filter is shown in Figure 3.2. The transmission properties of the used guide consisting of a dielectric rod with rectangular cross section, surrounded by several dielectrics of smaller refractive indices have been described by E. A. Marcatili [10].

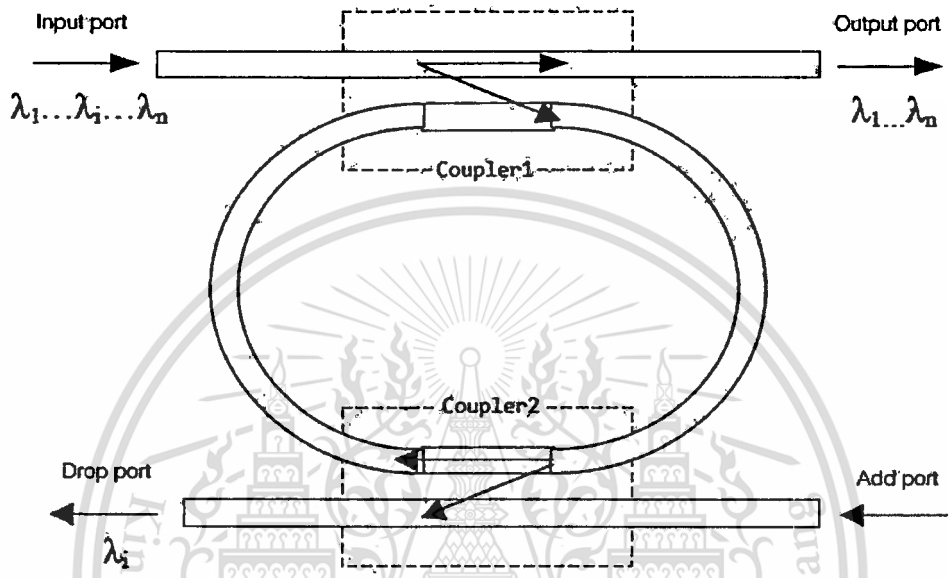

Figure 3.2 Ring resonator channel dropping filter.

A general architecture for an autoregressive planar waveguide optical filter was demonstrated for the first time in 1996 [11]. The autoregressive lattice filters which were designed and fabricated consisted of one and two stages using Ge-doped silica waveguides.

A signal flow chart transformation for evaluating the filter transfer functions was demonstrated. Purely passive single ring resonator filters as shown in Figure 3.1 have been realized in the material system AlGaAs-GaAs [12, 13] and Si-SiO_2 [14] and Si_3N_4- SiO_2 [15]. The radius of the used ring resonators is between 5 μm and 30 μm and the free spectral range (FSR) achieved is between 20 nm and 30 nm. Passive ring resonators in the form of a racetrack have been realized in the material system GaInAsP [16] and AlGaAs-GaAs [17]. The filter performance is limited by bending and scattering losses in the resonator. These losses could be compensated for by using an active material instead or in addition.

3.2 Optical Add/Drop Ring Resonator Filter

A ring resonator consists of a waveguide in a closed loop. The loop can be any closed shape, such as a circle, ellipse, or racetrack. The ring is placed near one or two bus waveguides (Figure 3.3). Typically, the input signal consists of one or more WDM channels. Signals on the input bus couple evanescently to the resonator. If a channel wavelength is resonant in the resonator, i.e., it encounters an integral multiple of 2π in phase over a round-trip, the signal intensity builds up in the ring, it couples to the output bus, and is "dropped." At the same time, a signal on the same wavelength can be added via the add port. The resonator thus functions as an add/drop multiplexer.

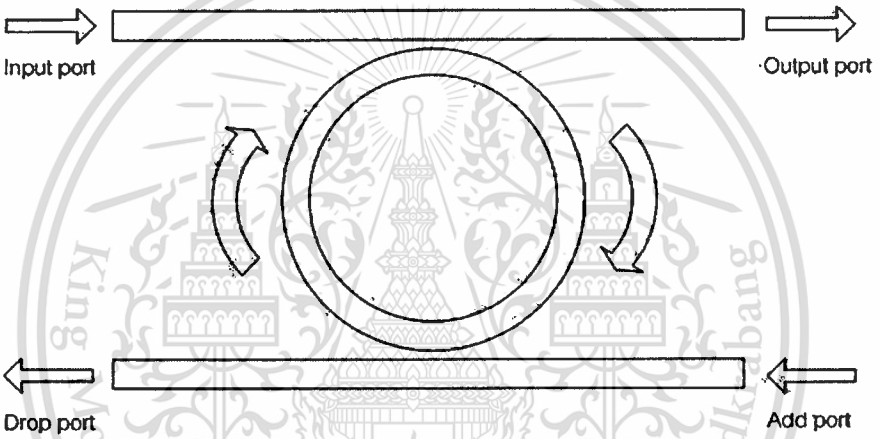

Figure 3.3 Schematic diagram for a ring resonator coupled to two waveguides as an add/drop filter.

An incident optical signal composed of multiple wavelengths ($\lambda_1,\ldots,\lambda_R,\ldots,\lambda_N$) at the input port coupled into the ring and for a resonant wavelength (λ_R), the energy builds up in the resonator despite the small coupling and eventually the signal is coupled into the drop port. Symmetrically, a new signal at resonant wavelength (λ_R') at the add port couples to the output port through the ring. As a result, such a configuration constitutes a very compact add/drop filter where a channel can be dropped from the WDM spectrum and replaced by a new signal on the same channel. Note that waves with a wavelength away from resonance will not repeat themselves in the ring and the coupled field interferes destructively with the wave in the resonator leading to little energy in the resonator and little dropped power. Residual dropped power at non-resonant wavelengths is possible due to imperfections and can induce inter-band crosstalk that is

detrimental to WDM applications. Moreover, if the input channel at λ_R is not completely extinguished, intra-band crosstalk will result. These issues will be studied and can be theoretically overcome by varying coupling parameters, inducing loss/gain in the ring and inserting additional rings between the two waveguides.

3.3 The Z-Transform Description

The filter functions arise from the interference of two or more waves that are delayed relative to each other. The incoming signal is split into multiple paths by a division of the wavefront or the amplitude. Diffraction gratings are an example of wavefront division, while directional couplers and partial reflectors are examples of amplitude division. After traveling along different paths, the fields are combined and interference occurs. For interference, the optical waves must have the same polarization, the same frequency and be temporally coherent over the longest delay length. When signals are recombined, their relative phases determine whether they interfere constructively or destructively. The phase Φ for each path is the product of the distance traveled, L and the propagation constant, β i.e., $\Phi = \beta L$ where $\beta = 2\pi n_e / \lambda$, which is expressed in terms of the refractive index n for a diffraction-based delay line or an effective index n_e for a waveguide delay line [18].

The individual optical path lengths are typically integer multiples of the smallest path length difference. The unit delay is defined as $T = L_u n / c$ where L_u is the smallest path length and is called the unit delay length. The refractive index is assumed to be independent of wavelength. The key to analyzing optical filters using Z-transforms is that each delay be an integer multiple of a unit delay length L_u. The phase for each path is then expressed as a multiple of βL_u, so $\Phi_p = p\beta L_u$, where p is an integer. The total transverse electric field for N paths is the sum over each optical path length given by

$$E_{out} = E_o e^{-j\Phi_0} + E_1 e^{-j\Phi_1} + E_2 e^{-j\Phi_2} + \ldots + E_{N-1} e^{-j\Phi_{N-1}} \quad (3.1)$$

To obtain a Z-transform of E_{out}, we express the phase as a multiple of the unit delay T. Using $\Omega = 2\pi\nu$ where $c = \nu\lambda$

$$\beta L_u = \frac{2\pi n L_u}{\lambda} = \frac{2\pi\nu n L_u}{c} = \frac{\Omega L_u n}{c} = \Omega T.$$

This gives $\Phi_p = p\beta L_u = p\Omega T$. Therefore Eq. 3.1 becomes,

$$E_{out} = E_o e^{-j0} + E_1 e^{-j\Omega T} + E_2 e^{-j2\Omega T} + \ldots + E_{N-1} e^{-j(N-1)\Omega T}. \quad (3.2)$$

For a dispersion-less line, unit delay T is a constant and using $z = e^{j\Omega T}$ in Eq. 3.2, we get

$$E_{out} = E_o + E_1 z^{-1} + E_2 z^{-2} + \ldots + E_{N-1} z^{-(N-1)}. \quad (3.3)$$

Because the delays are discrete multiples of the unit delay, the frequency response is periodic. One period is defined as the Free Spectral Range (FSR) and is given by $FSR = 1/T$. The normalized frequency $f = \omega/2\pi$ is related to the optical frequency by $f = (\nu - \nu_c)T$ or $f = (\Omega - \Omega_c)T/2\pi$. The center frequency $\nu_c = c/\lambda_c$ is defined so that the product of refractive index and unit length is equal to an integer number of center wavelengths, i.e., $m\lambda_c = nL_u$ where m is an integer. Propagation loss of a delay line is accounted for by multiplying z^{-1} by $x = e^{-\alpha L/2}$ where α is the average loss per unit length and L is the delay path length.

For a more realistic case for a delay line with dispersion, the FSR is given as:

$$FSR = 1/T = \frac{c}{n_g L_u}, \quad (3.4)$$

where $n_g = n_{eff} + f_o\left(dn_{eff}/df\right)_{f_o} = n_{eff} + \lambda_o\left(dn_{eff}/d\lambda\right)_{\lambda_o}$ is called as the *group refractive index* evaluated at either center frequency f_o or center wavelength λ_o.

The optical circuits are assumed to be linear and time invariant. They can be analyzed with Z-transforms using waveguide delays and directional couplers for splitting and combining signals. A schematic diagram of a directional coupler is shown in Figure 3.4. The lines in the figure indicate waveguides of finite width and height. Two waveguides are brought close together so that their evanescent fields overlap. A power coupling ratio κ is associated with each directional coupler. For an input on one port, the power coupled to the cross-port is κ times the input power. The length of the region where the waveguides are coupled determines the coupling ratio. The input output relation can be expressed using a 2x2 transfer matrix $\Phi_{cplr}(\kappa)$ as shown in Eq. 3.5, where κ is the power coupling ratio, and E_n^i and E_n^o, for n = 1, 2 represent the coupler input and output fields respectively.

The coupling ratio is assumed to be wavelength independent and hence the matrix elements are constants. The through and the cross-port transmission terms are given by $c = \cos\theta = \sqrt{(1-\gamma)(1-\kappa)}$ and $-js = -j\sin\theta = -j\sqrt{(1-\gamma)\kappa}$, respectively, where γ is the coupling

loss and θ is equal to the coupling strength integrated over the coupling length. A complex number $-j$ represents a $-(\pi/2)$ phase shift for the cross coupled light fields.

$$\begin{bmatrix} E_1^o \\ E_2^o \end{bmatrix} = \Phi_{cplr}(\kappa) \begin{bmatrix} E_1^i \\ E_2^i \end{bmatrix}, \quad \Phi_{cplr}(\kappa) = \begin{bmatrix} c & -js \\ -js & c \end{bmatrix}. \tag{3.5}$$

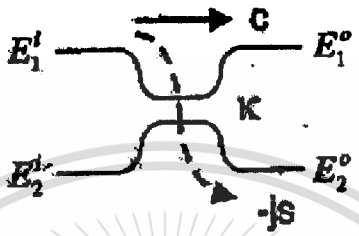

Figure 3.4 Directional coupler and I/O relations.

The basic filter structures require at least two paths for interference. The output is then the sum of each optical path. The transfer function from any input port to any output port can be written by inspection using the transmission of each path segment. The directional coupler transmission is given by $-js$ for the cross port and c for the through port. The transmission for each delay path is expressed in terms of the unit delay. A filter's transmission is then written by summing all paths between a particular input and output port.

3.3.1 Single Coupler Ring Resonator Filter (SCRR)

A ring resonator is simply a waveguide shaped into a ring structure as shown in Figure 3.5. To determine optical filter transfer function in Z-domain, the requirements of optical filters are considered to be satisfied are:

1) Linearity of all optical components.

2) Time invariance of all optical components.

3) Optical components must be lumped (i.e. not distributed).

The effects such as backscatter of light along the length of an optical fiber or waveguide, or saturation of an optical amplifier are therefore not considered here (the former is a distributed phenomenon; the latter is a nonlinear effect).

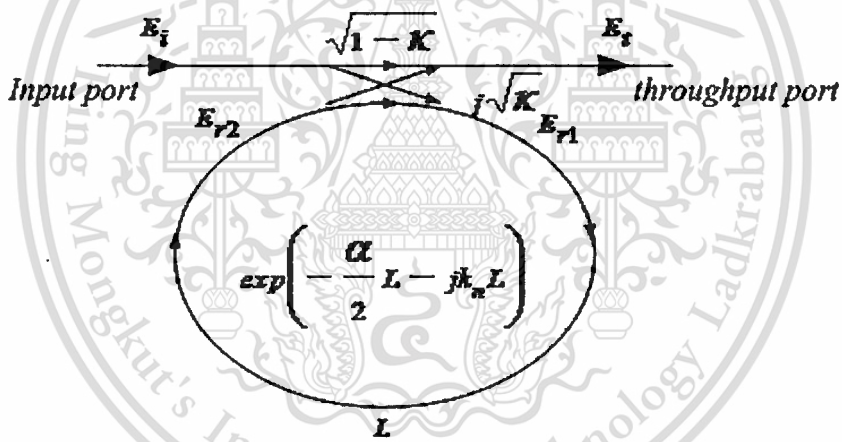

Figure 3.5 Schematic diagram for SCRR filter.

The transfer function of this configuration is derived using Z-transform analysis. The circumference of the ring is L ($L=2\pi R$, the radius is R), the coupling coefficient of the coupler is κ. The Z-transform parameter is represented by $z^{-1}=\exp^{-jk_nL}$ where $k_n=\frac{2\pi}{\lambda}n_{eff}$ is the propagation constant and n_{eff} is the effective index of the waveguide. The one round trip loss is $a=\exp^{-\alpha L/2}$, α is the intensity attenuation coefficient inside the waveguide [unit $length^{-1}$]. The transmitted or throughput field at the output of the straight waveguide, E_t and inserted electric field, E_i relations can be derived as followed:

$$E_t = (1-\gamma)^{1/2} \times \left[E_i \cdot \sqrt{1-\kappa} + j \cdot E_{r2} \sqrt{\kappa} \right] \tag{3.6}$$

$$E_{r1} = (1-\gamma)^{1/2} \times \left[j \cdot E_i \cdot \sqrt{\kappa} + E_{r2} \cdot \sqrt{1-\kappa} \right] \tag{3.7}$$

$$E_{r2} = E_{r1} \cdot a\, z^{-1}. \tag{3.8}$$

Using these equations, E_t / E_i can be calculated:

$$\frac{E_t}{E_i} = (1-\gamma)^{1/2} \times \left[\frac{\sqrt{1-\kappa} - (1-\gamma)^{1/2} \cdot a z^{-1}}{1 - (1-\gamma)^{1/2} \cdot \sqrt{1-\kappa} \cdot a z^{-1}} \right]. \tag{3.9}$$

The transfer function in Eq. (3.9) indicates that a ring resonator is very similar to a Fabry-Perot cavity. In the particular case shown in Figure 3.4, the corresponding Fabry-Perot cavity would have an input mirror with a field reflectivity and a fully reflecting output mirror. However, the field propagating inside the ring cavity is a traveling wave in contrast to the Fabry-Perot cavity which resonates a standing wave.

In the following, new parameter will be used for simplification:

$$\begin{aligned} D &= (1-\gamma)^{1/2} \\ x &= D \cdot \exp^{-\alpha L/2} \\ c &= \sqrt{1-\kappa} \\ \phi &= k_n \cdot L \end{aligned} \tag{3.10}$$

The intensity relation for the output port is given by:

$$T = \frac{I_t}{I_i}(\phi) = \left| \frac{E_t}{E_i} \right|^2 = D^2 \cdot \left[1 - \frac{(1-x^2) \cdot (1-c^2)}{(1-x \cdot c)^2 + 4 \cdot x \cdot c \cdot sin^2\left(\frac{\phi}{2}\right)} \right] \tag{3.11}$$

3.3.2 Double Coupler Ring Resonator Filter (DCRR)

Consider the architectures of double coupler ring resonator which sometime called add/drop filters as illustrated in Figure 3.6, which are constructed by 2×2 optical couplers.

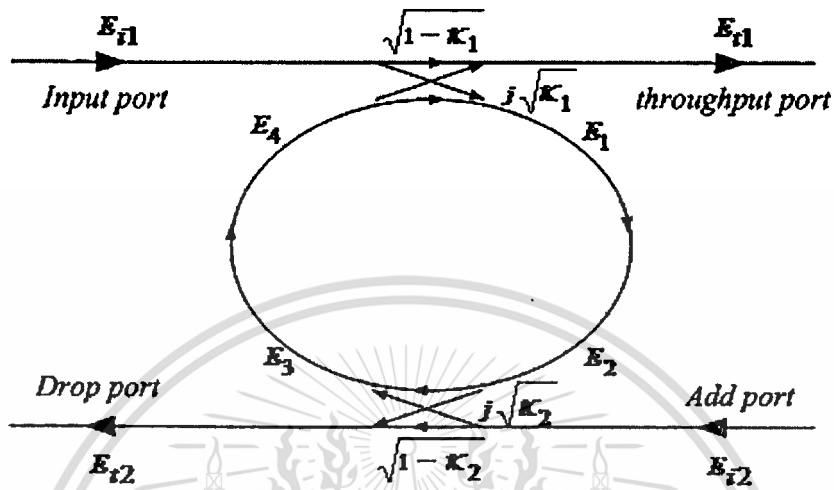

Figure 3.6 The architecture of DCRR or add/drop filter.

Similarly, the optical transfer functions of the ring resonator filters at the throughput port and drop port for an input port E_{i1} can be derived as followed. For the first coupler (κ_1), we have

$$E_{t1} = \sqrt{1-\gamma_1}\left[j\sqrt{\kappa_1}E_4 + \sqrt{1-\kappa_1}E_{i1} \right] \tag{3.12}$$

$$E_1 = \sqrt{1-\gamma_1}\left[j\sqrt{\kappa_1}E_{i1} + \sqrt{1-\kappa_1}E_4 \right] \tag{3.13}$$

where γ and κ_1 are the loss and the coupling coefficients, respectively. The incoming light of E_{i1} and E_4 are coupled through the first coupler to the output light E_{t1} and E_1 and the output light E_1 is transmitted through the ring becomes output light E_2. According to light transmission theory in linear optical systems, we obtain the following relation between E_1 and E_2

$$E_2 = E_1 e^{-\frac{\alpha L}{2}\frac{2}{2} - jk_n\frac{L}{2}} \tag{3.14}$$

where the transmission line length is $\frac{L}{2}$. The second coupler (κ_2) have the following relations:

$$E_{t2} = E_1 e^{-\frac{\alpha L}{2}\frac{2}{2} - jk_n\frac{L}{2}} \cdot j\sqrt{1-\gamma_2}\sqrt{\kappa_2} \qquad \text{at } E_{i2} = 0 \tag{3.15}$$

$$E_3 = E_1 e^{-\frac{\alpha L}{2\,2} - jk_n \frac{L}{2}} \sqrt{1-\gamma_2}\sqrt{1-\kappa_2} \tag{3.16}$$

Using the transmission theory, we obtain E_4 in terms of E_3

$$E_4 = E_3 e^{-\frac{\alpha L}{2\,2} - jk_n \frac{L}{2}} \tag{3.17}$$

$$E_1 = \frac{E_{i1} j\sqrt{1-\gamma_1}\sqrt{\kappa_1}}{1-\sqrt{1-\gamma_1}\sqrt{1-\kappa_1}\sqrt{1-\gamma_2}\sqrt{1-\kappa_2}e^{-\frac{\alpha}{2}L - jk_n L}} \tag{3.18}$$

$$E_4 = \frac{E_{i1} j\sqrt{1-\gamma_1}\sqrt{\kappa_1}}{1-\sqrt{1-\gamma_1}\sqrt{1-\kappa_1}\sqrt{1-\gamma_2}\sqrt{1-\kappa_2}e^{-\frac{\alpha}{2}L - jk_n L}} \sqrt{1-\gamma_2}\sqrt{1-\kappa_2}e^{-\frac{\alpha}{2}L - jk_n L} \tag{3.19}$$

By using the upper equations, the transfer function for throughput port and drop port in Figure 3.5 can thus be expressed as

Throughput port:

$$\begin{aligned}\frac{E_{t1}}{E_{i1}} &= \frac{-(1-\gamma_1)\kappa_1\sqrt{1-\kappa_2}e^{-\frac{\alpha}{2}L - jk_n L} + \sqrt{1-\gamma_1}\sqrt{1-\kappa_1}}{1-\sqrt{1-\gamma_1}\sqrt{1-\kappa_1}\sqrt{1-\gamma_2}\sqrt{1-\kappa_2}e^{-\frac{\alpha}{2}L - jk_n L}} \\ &= \frac{-(1-\gamma_1)(1-\kappa_1)\sqrt{1-\gamma_2}\sqrt{1-\kappa_2}e^{-\frac{\alpha}{2}L - jk_n L}}{1-\sqrt{1-\gamma_1}\sqrt{1-\kappa_1}\sqrt{1-\gamma_2}\sqrt{1-\kappa_2}e^{-\frac{\alpha}{2}L - jk_n L}} \\ &= \frac{-\sqrt{1-\gamma_2}\sqrt{1-\kappa_2}e^{-\frac{\alpha}{2}L - jk_n L} + \sqrt{1-\gamma_1}\sqrt{1-\kappa_1}}{1-\sqrt{1-\gamma_1}\sqrt{1-\kappa_1}\sqrt{1-\gamma_2}\sqrt{1-\kappa_2}e^{-\frac{\alpha}{2}L - jk_n L}}\end{aligned} \tag{3.20}$$

Drop port:

$$\frac{E_{t2}}{E_{i1}} = \frac{-\sqrt{1-\gamma_1}\sqrt{1-\gamma_2}\sqrt{\kappa_1\cdot\kappa_2}e^{-\frac{\alpha L}{2\,2} - jk_n \frac{L}{2}}}{1-\sqrt{1-\gamma_1}\sqrt{1-\kappa_1}\sqrt{1-\gamma_2}\sqrt{1-\kappa_2}e^{-\frac{\alpha}{2}L - jk_n L}} \tag{3.21}$$

The intensity relations for the throughput and drop port can be obtained by normalizing the transfer functions in Eqs. (3.20) and (3.21) which are given by

$$\frac{I_{t1}}{I_{i1}}=\left|\frac{E_{t1}}{E_{i1}}\right|^2=\frac{\begin{array}{c}1-(1-\gamma_1)\kappa_1-2\sqrt{1-\gamma_1}\sqrt{1-\kappa_1}\cdot\sqrt{1-\gamma_2}\sqrt{1-\kappa_2}e^{-\frac{\alpha}{2}L}cos(k_nL)\\ +(1-\gamma_2)(1-\kappa_2)e^{-\alpha L}\end{array}}{\begin{array}{c}1+(1-\gamma_1)(1-\kappa_1)\cdot(1-\gamma_2)(1-\kappa_2)e^{-\alpha L}\\ -2\sqrt{1-\gamma_1}\sqrt{1-\kappa_1}\cdot\sqrt{1-\gamma_2}\sqrt{1-\kappa_2}e^{-\frac{\alpha}{2}L}cos(k_nL)\end{array}} \tag{3.22}$$

$$\frac{I_{t2}}{I_{i1}}=\left|\frac{E_{t2}}{E_{i1}}\right|^2=\frac{(1-\gamma_1)(1-\gamma_2)\cdot\kappa_1\kappa_2e^{-\frac{\alpha}{2}L}}{\begin{array}{c}1+(1-\gamma_1)(1-\kappa_1)\cdot(1-\gamma_2)(1-\kappa_2)e^{-\alpha L}\\ -2\sqrt{1-\gamma_1}\sqrt{1-\kappa_1}\cdot\sqrt{1-\gamma_2}\sqrt{1-\kappa_2}e^{-\frac{\alpha}{2}L}cos(k_nL)\end{array}} \tag{3.23}$$

For simplification, the calculation of the intensity relation does not take into account coupling losses ($\gamma=0$) and the following parameters:

$$\begin{aligned}x&=exp\left(-\frac{\alpha}{2}L\right)\\ c_1&=\sqrt{1-\kappa_1}\\ c_2&=\sqrt{1-\kappa_2}\end{aligned} \tag{3.24}$$

The intensity relations Eqs. (3.22) and (3.23) are then given by

$$\frac{I_{t1}}{I_{i1}}(\phi)=\left|\frac{E_{t1}}{E_{i1}}\right|^2=1-\frac{\left(1-c_1^2\right)\cdot\left(1-c_2^2x^2\right)}{\left(1-c_1c_2x\right)^2+4c_1c_2xsin^2\left(\frac{\phi}{2}\right)} \tag{3.25}$$

$$\frac{I_{t2}}{I_{i1}}(\phi)=\left|\frac{E_{t2}}{E_{i1}}\right|^2=\frac{\left(1-c_1^2\right)\cdot\left(1-c_2^2\right)\cdot x}{\left(1-c_1c_2x\right)^2+4c_1c_2xsin^2\left(\frac{\phi}{2}\right)} \tag{3.26}$$

3.4 Enhanced Nonlinearity in Single Ring Resonator

In section 3.4 and 3.5, we will carefully study such enhancement and its projection on the dynamic performance of the microring resonator for all-optical switching applications. We will concentrate on the reduction achievable in the switching power of a microring due to the resonant condition.

For a small range of detuning, i.e., much smaller than the 3-dB bandwidth of the microring resonance, a small signal analysis approach is enough to understand the dynamic behavior of the resonator and to determine its switching enhancement. In such analysis, we will assume that the linear parameters of the microring resonator are constants with respect to time. Without loss of generality, we will consider the SCRR filter case in Figure 3.1 that we have introduced in section 3.3.1. At steady state, the field transmittance of the filter is given by

$$\frac{E_t}{E_i} = \frac{c - a e^{j\phi_0}}{1 - ca\, e^{j\phi_0}}. \tag{3.27}$$

where $a = \exp(-\alpha L/2)$ is the round trip field attenuation of the microring, c is the field transmittance coefficient, and $\phi_0 = \beta L$ is linear phase shift in the ring. β is the wave propagation constant associated with the fundamental mode supported by the ring waveguide, and L is the circumference of the ring. One useful feature of a ring resonator is that the original power gets to build up in the ring and keeps circulating inside the ring. The buildup factor B, which is defined as the ratio of the power circulating inside the ring to the input power, is given by [19]

$$B = \frac{P_r}{P_i} = \frac{1 - c^2}{1 + c^2 a^2 - 2ca\cos\phi_0} \tag{3.28}$$

where P_i is the input power, P_r is the average power inside the ring. Under conditions that the incident light is on resonance with the ring and the loss is negligible ($a = 1$), the maximum value of the buildup factor $B_{\max} = (1+c)/(1-c)$. Thus, when c is very close to unity, the power circulating inside the fiber ring becomes very high. This power buildup can induce nonlinear effects if the ring possesses an intensity-dependent nonlinear refractive index n_2 that results from the third-order susceptibility ($\chi^{(3)}$) of the waveguide material [19]. The nonlinear refractive index n_2 can be included in the single-pass phase shift as

$$\phi = \phi_0 + \phi_{NL} \cong \beta L + \gamma L_{eff} P_r \tag{3.29}$$

where $L_{eff} = [1 - \exp(-\alpha L)]/\alpha$, is the effective interaction length due to the loss and γ is the nonlinearity coefficient (related to n_2 by $\gamma = 2\pi n_2 / \lambda A_{eff}$, where λ is the input wavelength and A_{eff} is the effective core area of the waveguide). ϕ_0 and ϕ_{NL} are the single-pass linear and nonlinear phase shifts, respectively. In such a nonlinear case, ϕ_0 in Eq. (3.28) should now be replaced by ϕ. Thus, by substituting Eq. (3.29) into Eq. (3.28), we get a transcendental equation for the single-pass phase shift as

$$\phi(P_i, \phi_L) = \phi_L + \gamma L_{eff} \frac{1 - c^2}{1 + c^2 a^2 - 2ca\cos\phi(P_i, \phi_L)} P_i \tag{3.30}$$

The nonlinear response of switching device can be evaluated by the derivative of phase shift ϕ with respect to input power P_i. This derivative can be expressed as

$$\frac{d\phi}{dP_r} = \frac{d\phi}{d\phi_0}\frac{d\phi_0}{dP_r}\frac{dP_r}{dP_i} \approx \frac{8Ln_2}{\pi\lambda A_{eff}} F^2 \tag{3.31}$$

where F is resonator finesse [19].

3.5 Enhanced Nonlinearity in Add/Drop Ring Resonator

The transmission equation from input port to drop port for the DCRR as shown in Figure 3.6 is given by

$$\frac{E_{t2}}{E_{i1}} = \frac{s_1 s_2 \sqrt{\gamma} e^{j\phi_0}}{1 - c_1 c_2 \gamma e^{j\phi_0}} \tag{3.32}$$

where c_1, s_1 and c_2, s_2 are the coupling coefficients for the two couplers respectively. Critical coupling condition for the DCRR is defined to be $|E_{t2} / E_{i1}|^2 = 1$, i.e. all light goes through the drop port, which gives $s_{2c} = \sqrt{1 - c_1^2 e^{-\alpha L}}$. Since $s_{2c} = s_1$, symmetric DCRR (with two identical couplers) will operate at noncritical coupling. The phase shift of the drop port field (E_{t2}) is

$$\phi = \pi + \phi_0 + \arctan\left[\frac{c^2 \gamma \sin\phi_0}{1 - c^2 \gamma \cos\phi_0}\right] \tag{3.33}$$

Similar to SCRR, the nonlinear effect can be included by applying equation (3.29) to the computation of ϕ as follow.

$$\phi = \phi_0 + \frac{2\pi n_2 \frac{L}{2} P_2}{\lambda A_{eff}} + \frac{2\pi n_2 \frac{L}{2} P_4}{\lambda A_{eff}} \tag{3.34}$$

where P_2 and P_4 are circulating powers, respectively.

3.6 Ring Resonator Operation

The transfer of power between the two port waveguides of a four port micro-resonator is only possible at discrete wavelength regions at which the optical path length of the light in the resonator is an integer multiple of its effective wavelength.

The process by which power is transferred through the resonator is characterized by three distinct phases: the initial, transient and Steady State as shown in Figures 3.7.

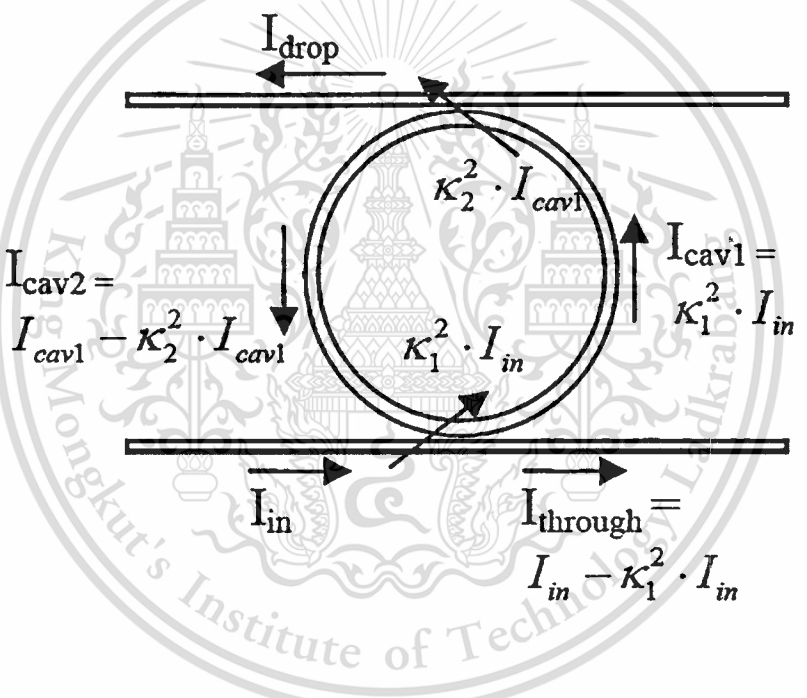

Figures 3.7 The process by which power is transferred through the ring resonator.

The Initial State

- Incoming light I_{in} of a certain wavelength propagates along one of the port waveguides of the micro-resonator.
- When the light reaches the first coupler a small power fraction $K_1^2 \cdot I_{in1}$ is evanescently coupled into the resonator.
- Most of the light, however, will continue its path along the port waveguide as $I_{through}$ The light I_{cav1} that is now in the resonator will propagate along the resonator until it reaches the other port waveguide and the second coupler.
- Here a small fraction $K_2^2 \cdot I_{cav1}$ of the light is coupled out of the resonator as I_{drop} while the larger fraction I_{cav2} continues its roundtrip towards the first coupler.

The Transient State

- In the transient phase the dominant factor that determines the buildup of power the resonator is the modal phase of the light I_{cav2} as it interferes with the light in the port waveguide at the first coupler.
- If the resonance condition $\phi_r = m \cdot 2\pi, m \epsilon N$ is satisfied for the roundtrip phase of I_{cav2} , constructive interference will occur at the resonator side of the first coupler, resulting in a net increase of power within the resonator.
- At the same time destructive interference at the port waveguide side results in a decrease of the power $I_{through}$.

The Steady State

- The process of power enhancement within the cavity while transferring more power from I_{in} will repeat itself many times as I_{cav2} continues to interfere with the light in the port waveguide on every round-trip.

- The intra-cavity power cannot rise indefinitely, however, and at a certain power level a state of equilibrium is reached between the light I_{cav2} in the cavity and the light in the port waveguide I_{in}.

- At this point no additional power can be transferred from I_{in} and the resonator is operating in a steady state condition. The power in the through port $I_{through}$ is now at its lowest level while the power in the drop port I_{drop} is at its highest level. The resonator has thus effectively transferred power from the input to the drop port.

CHAPTER 4

ENHANCEMENT OF FREE SPECTRAL RANGE USING RING RESONATORS

4.1 Free Spectral Range Generation

Light from a monochromatic light source is launched into a ring resonator with constant light field amplitude (E_0) and random phase modulation, which is the combination of terms in attenuation (α) and phase (ϕ_0) constants, which results in temporal coherence degradation. Hence, the time dependent input light field (E_{in}), without pumping term, can be expressed as

$$E_{in}(t) = E_0 exp^{-\alpha L + j\phi_0(t)}. \tag{4.1}$$

where L is a propagation distance (waveguide length).

We assume that the nonlinearity of the optical ring resonator is of the Kerr-type, i.e., the refractive index is given by

$$n = n_0 + n_2 I = n_0 + \left(\frac{n_2}{A_{eff}}\right) P, \tag{4.2}$$

where n_0 and n_2 are the linear and nonlinear refractive indexes, respectively. I and P are the optical intensity and optical power, respectively. The effective mode core area of the device is given by A_{eff}. For the microring and nanoring resonators, the effective mode core areas range from 0.10 to 0.50 μm^2 [20].

When a Gaussian pulse is input and propagated within a ring resonator as shown in Figure 4.1, which consists of series microring resonators and nanoring resonator. The resonant output is formed, thus, the normalized output of the light field is the ratio between the output and input fields ($E_{out}(t)$ and $E_{in}(t)$) in each roundtrip, which can be expressed as [21]

$$\left|\frac{E_{out}(t)}{E_{in}(t)}\right|^2 = (1-\gamma)\left[1 - \frac{(1-(1-\gamma)x^2)\kappa}{\left(1-x\sqrt{1-\gamma}\sqrt{1-\kappa}\right)^2 + 4x\sqrt{1-\gamma}\sqrt{1-\kappa}\sin^2\left(\frac{\emptyset}{2}\right)}\right] \quad (4.3)$$

An equation (4.3) indicates that a ring resonator in the particular case is very similar to a Fabry-Perot cavity, which has an input and output mirror with a field reflectivity, $(1-\kappa)$, and a fully reflecting mirror. κ is the coupling coefficient, and $x = \exp(-\alpha L/2)$ represents a roundtrip loss coefficient, $\phi_0 = kLn_0$ and $\phi_{NL} = kL\left(\frac{n_2}{A_{eff}}\right)P$ are the linear and nonlinear phase shifts, $k = 2\pi/\lambda$ is the wave propagation number in a vacuum. Where L and α are a waveguide length and linear absorption coefficient, respectively. In this work, the amplified signals with constant output and without the change in phase are required to confirm the large bandwidth output. Therefore, the iterative method is introduced to obtain the results as shown in equation (3), similarly, when the output field is connected and input into the other ring resonators.

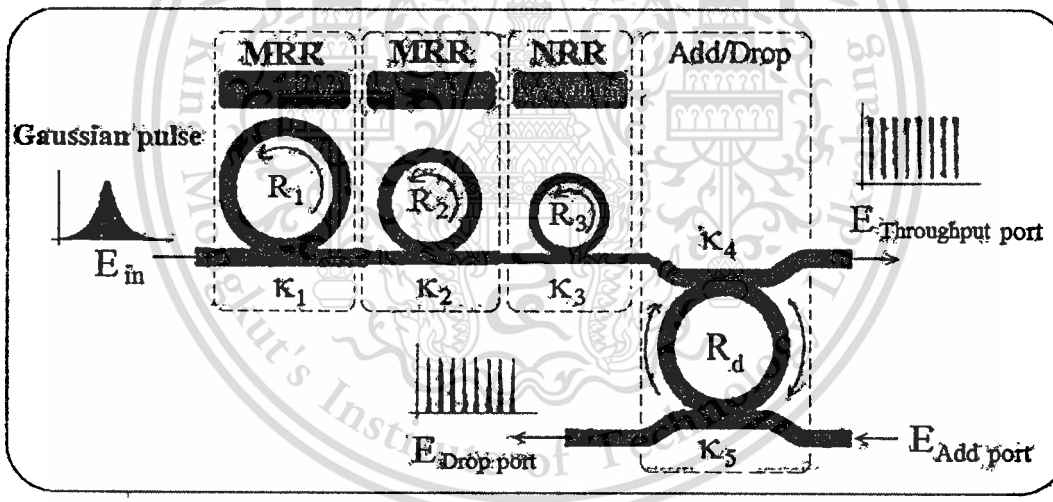

Figure 4.1 A schematic of a Gaussian soliton generation system.

The input optical field as shown in equation (4.1), i.e. a Gaussian pulse, is input into a nonlinear microring resonator. By using the appropriate parameters, the chaotic signal is obtained by using the appropriate parameters in equation (4.3). To retrieve the signals from the chaotic noise, we propose to use the add/drop device with the appropriate parameters. This is given in details as followings. The optical outputs of a ring resonator add/drop filter can be given by the equations (4.4) and (4.5) [21,22].

$$\left|\frac{E_t}{E_{in}}\right|^2 = \frac{(1-\kappa_1)-2\sqrt{1-\kappa_1}\cdot\sqrt{1-\kappa_2}e^{-\frac{\alpha}{2}L}\cos(k_n L)+(1-\kappa_2)e^{-\alpha L}}{1+(1-\kappa_1)(1-\kappa_2)e^{-\alpha L}-2\sqrt{1-\kappa_1}\cdot\sqrt{1-\kappa_2}e^{-\frac{\alpha}{2}L}\cos(k_n L)} \quad (4.4)$$

and

$$\left|\frac{E_d}{E_{in}}\right|^2 = \frac{\kappa_1\kappa_2 e^{-\frac{\alpha}{2}L}}{1+(1-\kappa_1)(1-\kappa_2)e^{-\alpha L}-2\sqrt{1-\kappa_1}\cdot\sqrt{1-\kappa_2}e^{-\frac{\alpha}{2}L}\cos(k_n L)} \quad (4.5)$$

where E_t and E_d represents the optical fields of the throughput and drop ports respectively. The transmitted output can be controlled and obtained by choosing the suitable coupling ratio of the ring resonator, which is well derived and described by reference [21]. Where $\beta = kn_{eff}$ represents the propagation constant, n_{eff} is the effective refractive index of the waveguide, and the circumference of the ring is $L = 2\pi R$, here R is the radius of the ring. In the following, new parameters will be used for simplification, where $\phi = \beta L$ is the phase constant. The chaotic noise cancellation can be managed by using the specific parameters of the add/drop device, which the required signals at the specific wavelength band can be filtered and retrieved. κ_1 and κ_2 are coupling coefficient of add/drop filters, $k_n = 2\pi/\lambda$ is the wave propagation number for in a vacuum, and the waveguide (ring resonator) loss is α = 0.5 dBmm^{-1}. The fractional coupler intensity loss is γ = 0.1. In the case of add/drop device, the nonlinear refractive index is neglected.

4.2 Enhancement of Free Spectral Range

From Figure 4.1, in principle, light pulse is sliced to be the discrete signal and amplified within the first ring, where more signal amplification can be obtained by using the smaller ring device (second ring). Finally, the required signals can be obtained via a drop port of the add/drop filter. In operation, an optical field in the form of Gaussian pulse from a laser source at the specified center wavelength is input into the system. In practice, the maximum frequency that can be confined within the optical waveguide has been increased by using the composite of materials known as meta-materials [23].

From Figure 4.2, the Gaussian pulse with center wavelength at 1.55 μm, pulse width (Full Width at Half Maximum, FWHM) of 20 ns, peak power at 2 W is input into the system as shown in Figure 4.2(a). The suitable ring parameters are used, for instance, ring radii R_1 = 15.0 μm, $R_2 = R_3$ = 9.0 μm, and $R_d = R_4$ = 50.0 μm. In order to make the system associate with the practical device [20,24], the selected parameters of the system are fixed to n_0 = 3.34 (InGaAsP/InP), A_{eff} = 0.50 μm^2 and 0.25 μm^2 for a microring and add/drop ring resonator, respectively, α = 0.5 dBmm^{-1}, γ = 0.1. In this investigation, the coupling coefficient (kappa, κ) of the microring resonator is ranged from 0.10 to 0.96. The nonlinear refractive index of the microring used is $n_2 = 2.2 \times 10^{-17}$ m^2/W.

In this case, the attenuation of light propagates within the system (i.e. waveguided) used is 0.5 dBmm^{-1}. After light is input into the system, the Gaussian pulse is chopped (sliced) into a smaller signal spreading over the spectrum due to the nonlinear effects [22], the large bandwidth signal is generated within the first ring device, which is shown in Figure 4.2(b). In applications, the specific input or output frequencies can be used and generated, where the suitable parameters are used and shown in the figure. The similar manner is as shown in Figures 4.3 - 4.7, where the different parameters are the R_d radii and coupling coefficients (kappa, κ), where the small FSR is obtained.

In application, the use of the generated frequency band for up-down link for wireless link is employed. Furthermore, there are several frequency bands available as shown in Figures 4.2 - 4.7, which can be brought the high capacity channels and multi switching system in the MANET system, which have shown in conclusion.

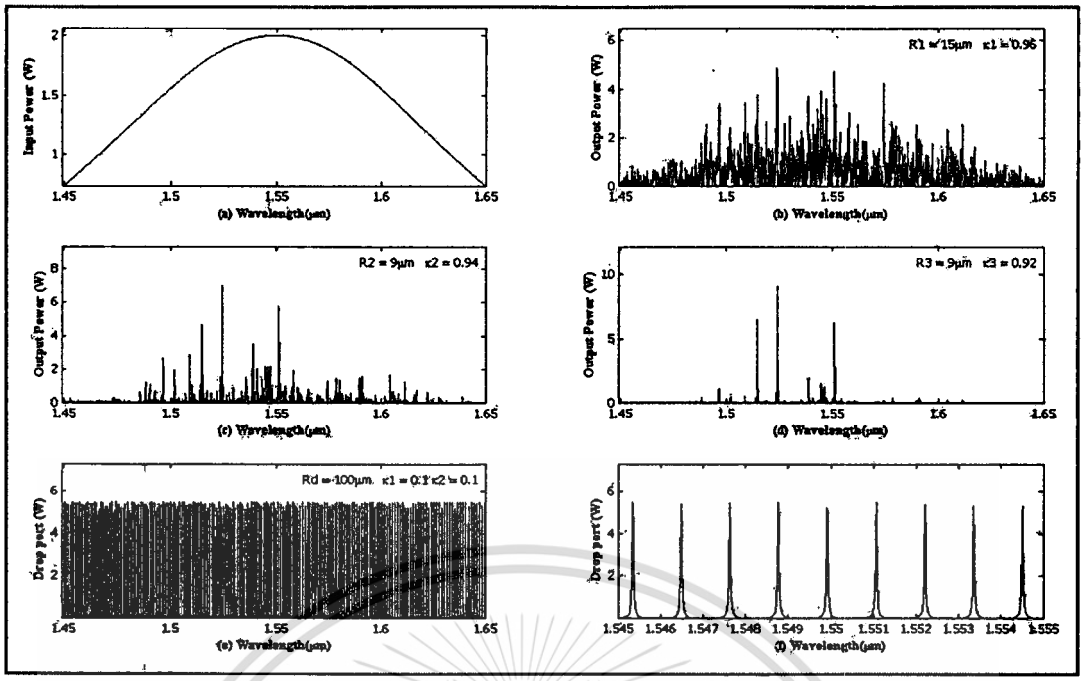

Figure 4.2 Center wavelength at 1.55 μm, where (a) the input Gaussian pulse, (b) the large bandwidth signal, (c) and (d) are the filtering and amplifying signals, (e) and (f) are the drop port signals, with $R_d = 100\ \mu m$.

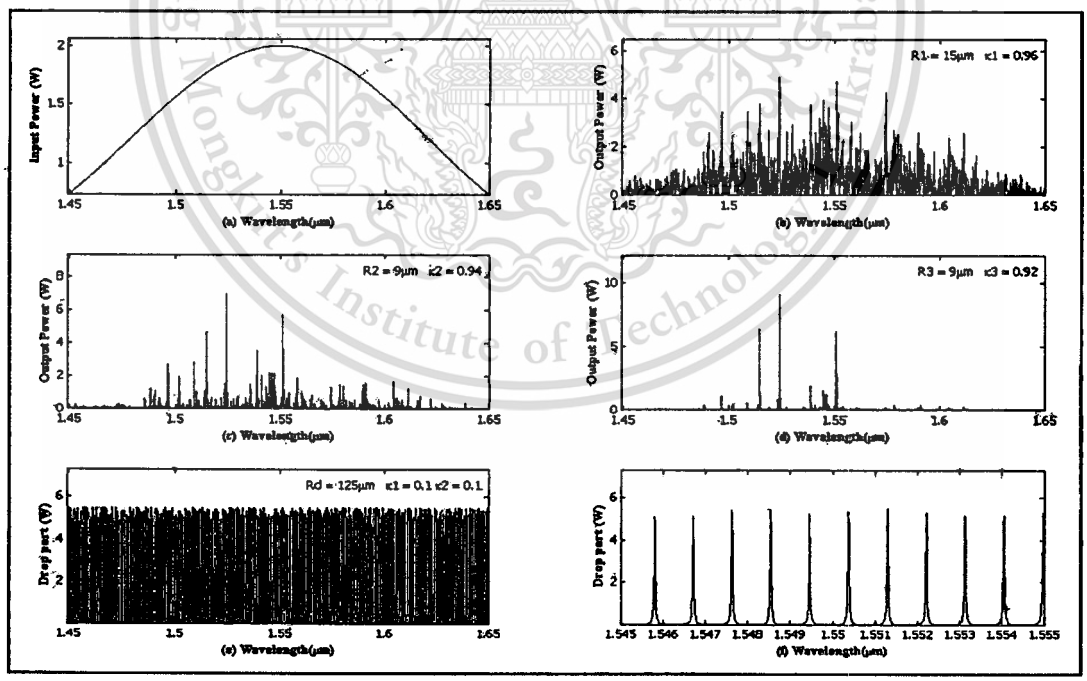

Figure 4.3 Center wavelength at 1.55 μm, where (a) the input Gaussian pulse, (b) the large bandwidth signal, (c) and (d) are the filtering and amplifying signals, (e) and (f) are the drop port signals, with $R_d = 125\ \mu m$.

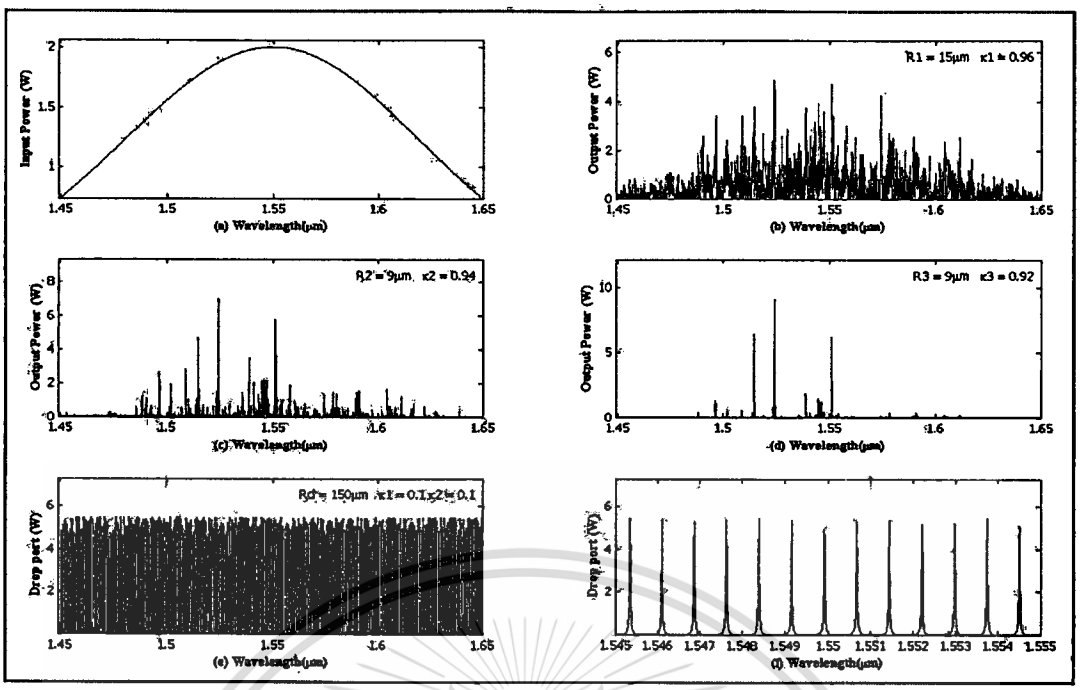

Figure 4.4 Center wavelength at 1.55 μm, where (a) the input Gaussian pulse, (b) the large bandwidth signal, (c) and (d) are the filtering and amplifying signals, (e) and (f) are the drop port signals, with $R_d = 150\ \mu m$.

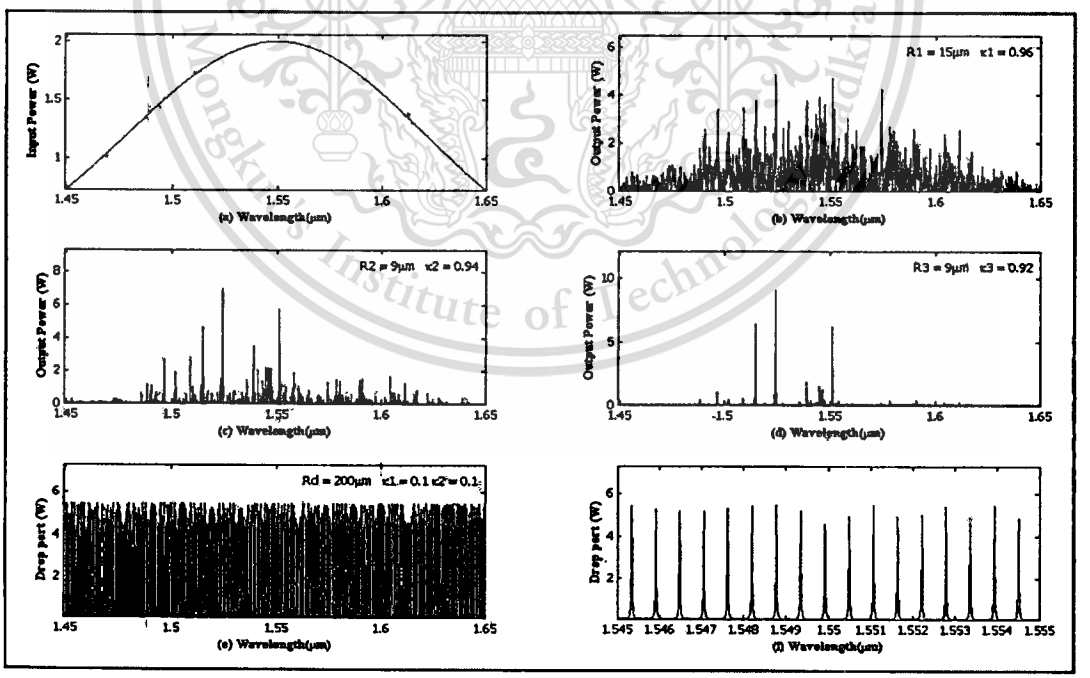

Figure 4.5 Center wavelength at 1.55 μm, where (a) the input Gaussian pulse, (b) the large bandwidth signal, (c) and (d) are the filtering and amplifying signals, (e) and (f) are the drop port signals, with $R_d = 200\ \mu m$.

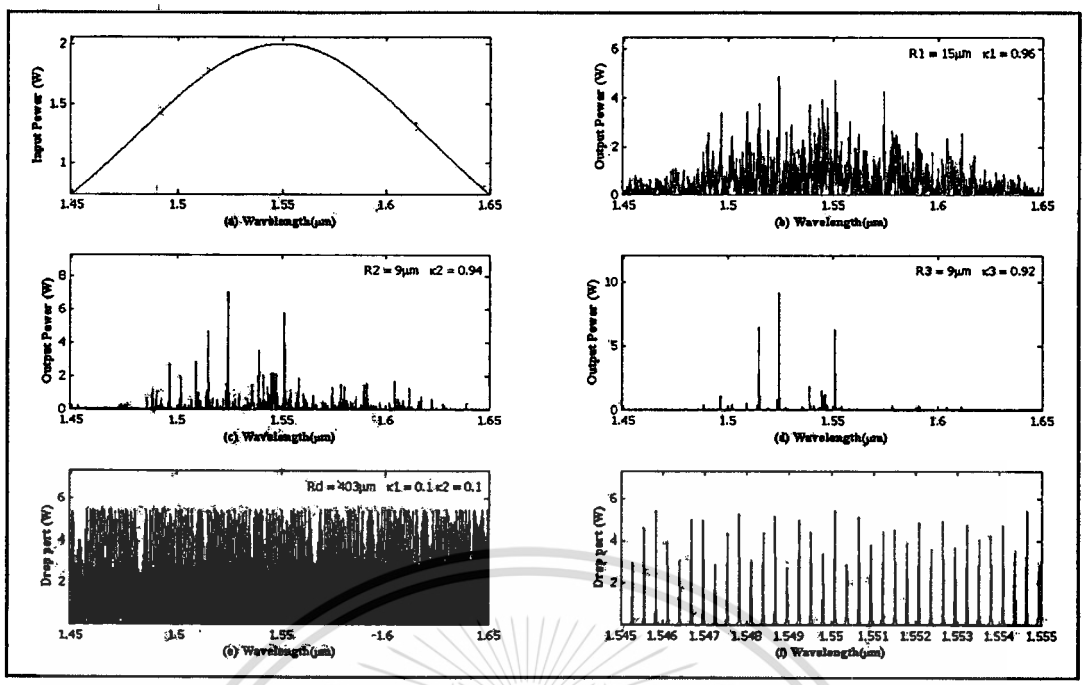

Figure 4.6 Center wavelength at 1.55 μm, where (a) the input Gaussian pulse, (b) the large bandwidth signal, (c) and (d) are the filtering and amplifying signals, (e) and (f) are the drop port signals, with $R_d = 403\ \mu m$.

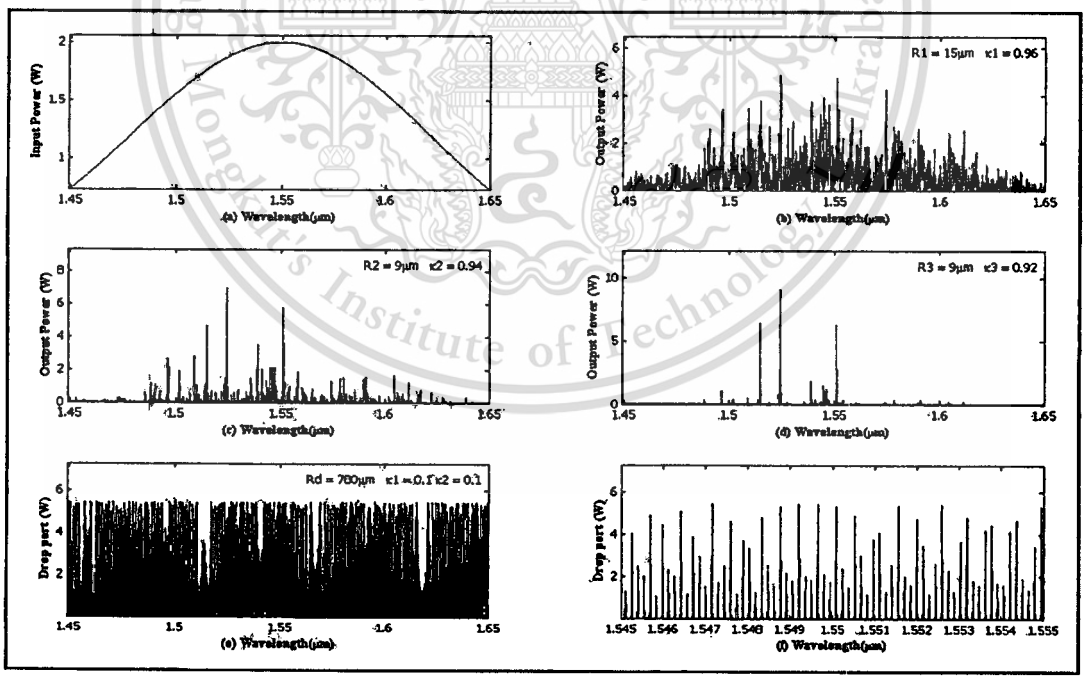

Figure 4.7 Center wavelength at 1.55 μm, where (a) the input Gaussian pulse, (b) the large bandwidth signal, (c) and (d) are the filtering and amplifying signals, (e) and (f) are the drop port signals, with $R_d = 780\ \mu m$.

To verify that results of this system. I had compared a FSR of drop port signals with FSR from reference [25] as shown in Table 4.1.

R_d	FSR of this thesis	FSR from reference [25]
100	1.1	5.2
200	0.68	3.2
403	0.28	2.0
780	0.15	1.0

Table 4.1 A FSR of this thesis compared with FSR from reference [25].

From table 4.1 can be conclude a FSR that decrease when ring radius of add/drop filter (R_d) is increasing and can be plotted a FSR as shown in Figures 4.8. When compare a FSRs of this thesis with FSRs from reference [25] that are give a narrow FSR more than from reference.

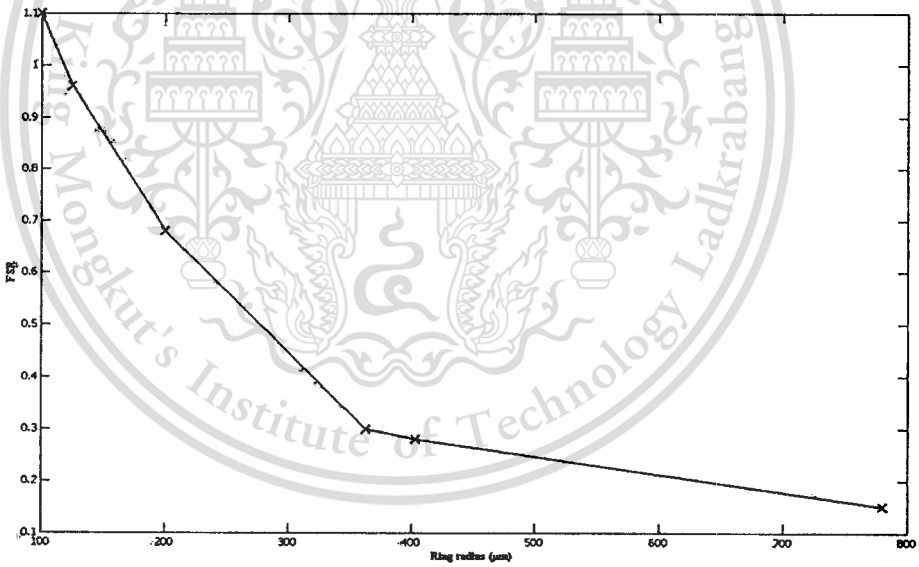

Figures 4.8 Plot FSRs that depend on Ring radii.

4.3 Summary

I have shown that the multi frequency bands generated by using a Gaussian pulse with center wavelength at 1.55 μm propagating within the microring resonator system. The large bandwidth signal is generated within the first microring resonator and amplified via second microring and nanoring resonator. To select or add the specific signal, it done by using add/drop filter. So the results of output signal at the drop port, where used the different parameters are the R_d radii and the same coupling coefficients (kappa, κ) have been shown in Figures 4.2(f) - 4.5(f). Those results have shown the increasing of channel capacity and the small FSR is obtained. But all the defined parameters must depend on the real fabrication.

CHAPTER 5

CONCLUSIONS

A study of an Optical Pulse in nonlinear device has been proposed. This study is application to all-optical signal processing. The system consists of single and add/drop ring resonator can be generated or multiplexed the large bandwidth signal with the signal in the transmission system. The required signals can be filtered by the add/drop device, where the coupling coefficients (κ) are the main parameter to made the optical output signal at the throughput and drop port. The cancellation of signal with the wavelength (λ_i) carrier can be performed and selected from the drop port. The optical output signal has been shown the small FSR also multi frequency bands can be generated by using a Gaussian pulse. Which increasing a channel capacity and signal security and can be applied to the optical communication systems and secured data transmission.

5.1 Future work

For future work of this thesis that can be integrated the proposed system with the cellular wireless or MANET network, which can be simultaneous up/down link [24] within a single device and available for the extended multi switching application with the frequency center at the THz band as shown in Figures 5.1-5.2.

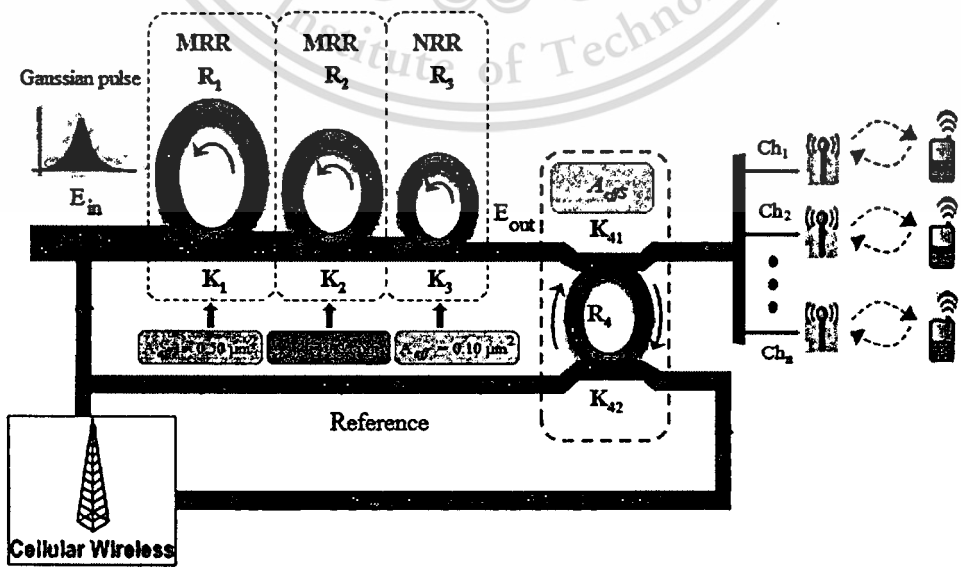

Figure 5.1 A schematic of a cellular wireless integrated with optical device system.

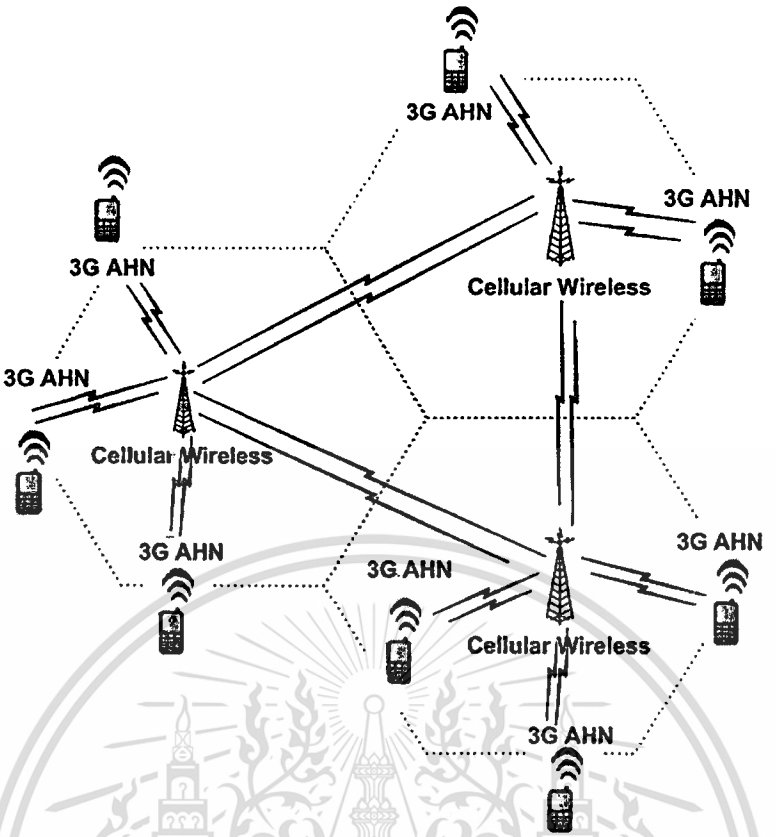

Figure 5.2 A schematic diagram of MANET surveillance model.

The higher channel capacity can also be obtained by using FSR modification and more available frequency bands, for instance, the use of system different parameters can provide more frequency bands as shown in Figures 4.2 - 4.5. The generated carrier signals can be used as the modulated carrier that can be used to form the simultaneous up and down link and multi switching, which is controlled by a computer server. This can also be used with the existed public network installation or Ad Hoc network applications. Furthermore, the pumping part is not required in such a system. The new available frequency bands can be use to form the new multi-frequency layer protocol, where more communication capacity can be performed.

LIST OF PUBLICATION

1. **C. Sirawattananon**, S. Mitatha, P. Bunyatnoparat, S. Punthawanunt and P.P. Yupapin, **"A Proposal of a High Resolution Tunable Visible Laser Source Generation"**, The 9th International Symposium on Communications And Information Technology (ISCIT), 2009. pp. 1235-1236

A Proposal of a High Resolution Tunable Visible Laser Source Generation

C. Sirawattananon[1], S. Mitatha[1], P. Bunyatnoparat[1], S. Punthawanunt[2] and P.P. Yupapin[3]
[1]Hybrid Computing Research Laboratory, Faculty of Engineering
King Mongkut's Institute of Technology Ladkrabang, Bangkok 10520, Thailand
[2]Faculty of Science and Technology
Kasem Bundit University, Bangkok 10250, Thailand
[3]Advanced Research Center for Photonics, Faculty of Science
King Mongkut's Institute of Technology Ladkrabang, Bangkok 10520, Thailand
E-mail: kmsomsak@kmitl.ac.th

Abstract— **A new system of a highly tunable visible laser source using a Gaussian pulse propagating within a nonlinear microring resonator system is proposed. Several Gaussian pulses with different center wavelengths are investigated using the designed system. The obtained results have shown that the very fine tuning wavelengths cover the visible laser wavelengths can be generated. With the very sharp peak and broad spectrum, for instance, when the Gaussian input pulse with the center wavelength at 700 nm, the spectral width of 20 nm is obtained. The interesting aspect is that the increasing in microscopic recording pen (i.e. peak) can be used to increase the imaging resolution, where the multi-color imaging, especially, for multi-color bio-cell microscopy is the target.**

I. INTRODUCTION

A new 'visible laser', which is based on a very simple design could be tailor-made to instantly detect the presence of particular molecules or cells, for example poisons or explosives in transport screening situations, or proteins in patients' blood samples, with high resolution. In principle, the visible laser wavelength can be extended to cover the broader wavelength with very fine tuning spectral width, which can be used to increase the imaging resolution. By using a common laser input into the proposed nonlinear device system, the extended wavelength with power amplification can be achieved. However, many earlier visible laser investigations have been reported [1-5], which is capable ranging from visible to near-infrared region [6]. Recently, the use of a tiny device known as a microring resonator in various application has been reported [7, 8]. They found that the broad spectrum of light pulse can be transformed to the discrete pulses. Therefore, in this work we are looking for a common laser source that can be used to form the broad output spectra. The use of a Gaussian pulse to form a broad band wavelength within a nonlinear microring resonator system is recommended.

II. LASER SOURCE GENERATION

The specific wavelength of light source can be generated by using the simple device schematic diagram as shown in Fig. 1. Light from a monochromatic light source is launched into a nonlinear microring resonator system with constant light field amplitude (E_0) and random phase modulation (ϕ_0). Hence, the time dependent input light field (E_{in}) can be expressed as

$$E_{in}(t) = E_0 \exp^{j\phi_0(t)}. \quad (1)$$

We assume that the nonlinearity of the optical ring device is of the Kerr-type, i.e., the refractive index is given by

$$n = n_0 + n_2 I = n_0 + \left(\frac{n_2}{A_{eff}}\right)P, \quad (2)$$

where n_0 and n_2 are the linear and nonlinear refractive indexes, respectively. I and P are the optical intensity and optical power, respectively. The effective mode core area of the device is given by A_{eff}. For the microring and nanoring resonators, the effective mode core areas range from 0.10 to 0.50 μm^2 [9].

When a Gaussian pulse is input and propagated within a microring resonator as shown in Fig. 1, which consists of series microring resonators. The resonant output is formed, thus, the normalized output of the light field is the ratio between the output and input fields ($E_{out}(t)$ and $E_{in}(t)$) in each roundtrip, which can be expressed as [7].

$$\left|\frac{E_{out}(t)}{E_{in}(t)}\right|^2 = (1-\gamma)\left[1 - \frac{(1-(1-\gamma)x^2)\kappa}{(1-x\sqrt{1-\gamma}\sqrt{1-\kappa})^2 + 4x\sqrt{1-\gamma}\sqrt{1-\kappa}\sin^2\left(\frac{\phi}{2}\right)}\right] \quad (3)$$

An equation (3) indicates that a ring resonator in the particular case is very similar to a Fabry-Perot cavity, which has an input and output mirror with a field reflectivity, $(1-\kappa)$, and a fully reflecting mirror. κ is the coupling coefficient, and $x = \exp(-\alpha L/2)$ represents a roundtrip loss coefficient,

$\phi_0 = kLn_0$ and $\phi_{NL} = kLn_2|E_{in}|^2$ are the linear and nonlinear phase shifts, $k = 2\pi/\lambda$ is the wave propagation number in a vacuum. Where L and α are a waveguide length and linear absorption coefficient, respectively. To filter the required signals from the Gaussian band, we propose to use the add/drop device. The optical outputs of a ring resonator add/drop filter can be given by the equations (4) and (5) [8].

$$\left|\frac{E_t}{E_{in}}\right|^2 = \frac{(1-\kappa_1)-2\sqrt{1-\kappa_1}\cdot\sqrt{1-\kappa_2}\,e^{-\frac{\alpha_2}{2}}\cos(k_n L)+(1-\kappa_2)e^{-\alpha L}}{1+(1-\kappa_1)(1-\kappa_2)e^{-\alpha L}-2\sqrt{1-\kappa_1}\cdot\sqrt{1-\kappa_2}\,e^{-\frac{\alpha_2}{2}}\cos(k_n L)} \quad (4)$$

$$\left|\frac{E_d}{E_{in}}\right|^2 = \frac{\kappa_1\kappa_2 e^{-\frac{\alpha_2}{2}}}{1+(1-\kappa_1)(1-\kappa_2)e^{-\alpha L}-2\sqrt{1-\kappa_1}\cdot\sqrt{1-\kappa_2}\,e^{-\frac{\alpha_2}{2}}\cos(k_n L)} \quad (5)$$

Where E_t and E_d represents the optical fields of the throughput and drop ports respectively. Where $\beta = kn_{eff}$ represents the propagation constant, n_{eff} is the effective refractive index of the waveguide, and the circumference of the ring is $L = 2\pi R$, where $\phi = \beta L$ is the phase constant. κ_1 and κ_2 are coupling coefficient of add/drop filters, $k_n = 2\pi/\lambda$ is the wave propagation number for in a vacuum, and the waveguide (ring resonator) loss is α = 0.5 dBmm^{-1}. The fractional coupler intensity loss is γ = 0.1.

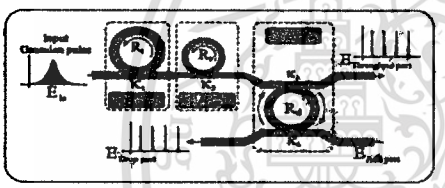

Fig. 1. A schematic of a Gaussian pulses generation system, where R_n: ring radii, κ_n: coupling coefficients, R_d : an add/drop ring radius, A_{eff}: Effective areas.

An optical field in the form of Gaussian pulse with 20 ns pulse width, peak power at 2 W is input into the system. The large bandwidth signals can be seen within the second microring device, and shown in Fig. 2(a).

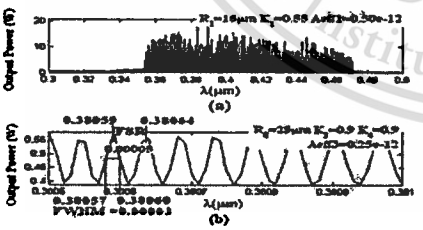

Fig. 2. Result of the spatial pulses with center wavelength at 400 nm, where (a) large bandwidth signals, (b) filtering and amplifying signals from the drop port.

III. Conclusions

We have shown that the multi-color laser wavelengths can be generated by using a Gaussian pulse propagating within the microring resonator system, which is available for the extended visible laser wavelengths. By using the center wavelengths at 400, 600 and 700 nm, the obtained results have shown that visible laser wavelength can be generated, where the smallest spatial pulse width of 20 nm with the spectrum range of 50 fm can be generated and achieved. Furthermore, the Gaussian pulse power can be amplified, which can provide the powerful laser source for wider applications. We find that the maximum power of 150 W can be obtained, however, the coupling coefficient of the add/drop filter is the major parameter of the required coupling output power. In applications, the use of wider wavelengths of visible lasers may be useful for multi-color imaging with very high resolution, especially, for multi-color holographic recording and imaging applications.

References

[1] Y. Feng, S. Huang, A. Shirakawa, and Ken-ichi Ueda, "Multiple-color cw visible lasers by frequency sum-mixing in a cascading Raman fiber laser," Opt. Exp., 12(9)(2004)1843-1847.

[2] H. Watanabe, T. Omatsu and M. Tateda, "Efficient self-pumped phase conjugation with a loop geometry in a Rhodamine-6G solid dye laser amplifier," Opt. Exp., 11(2003)176-180.

[3] J. C. Bienfang, C. A. Denman, B. W. Grime, P. D. Hillman, G. T.Moore and J. M. Telle, "20 W of continuous-wave sodium D2 resonance radiation from sum-frequency generation with injection-locked lasers," Opt. Lett., 28(2003)2219-2221.

[4] G. Z. Luo, S. N. Zhu, J. L. He, Y. Y. Zhu, H. T. Wang, Z. W. Liu, C. Zhang and N. B. Ming, "Simultaneously efficient blue and red light generations in a periodically poled LiTaO3," Appl. Phys. Lett. 78(2001)3006-3008.

[5] R. P. Mildren, M. Convery, H. M. Pask, J. A. Piper and T. Mckay, "Efficient, all-solid-state, Raman laser in the yellow, orange and red," Opt. Exp., 12(2004)785-790.

[6] K.J. Jyoti, H. Mattoussi, J. M. Mauro, S.M. Simon, "Long-term multiple color imaging of live cells using quantum dot bioconjugates," Nature Biotechnology, 21(2002)47-51.

[7] N. Pornsuwancharoen and P.P. Yupapin, "Generalized fast, slow, stop, and store light optically within a nanoring resonator," Microw. and Opt. Technol. Lett., 51(2009) 899-902.

[8] P.P. Yupapin, P. Saeung and C. Li, "Characteristics of complementary ring-resonator add/drop filters modeling by using graphical approach," Opt. Commun., 272(2007)81-86.

[9] Y. Su, F. Liu and Q. Li, "System performance of slow-light buffering and storage in silicon nano-waveguide," Proc. SPIE, 6783(2007)68732P.

REFERENCES

[1] Govind P.Agrawal. Lightwave technology : telecommunication systems. Hoboken, NJ : John Wiley, 2005.

[2] Milorad cvijetic. Optical transmission systems engineering. Boston : Artech House, 2004.

[3] Rajiv Ramaswami, Kumar N. Sivarajan. Optical Network : A Practical Perspective. 2nd ED. San Francisco, CA : Morgan Kaufmann, 2002.

[4] Govind P. Agrawal. Fiber-Optic Communication Systems. 2nd ED. New York : John Wiley, 1997.

[5] J. Kani et al. Interwavelength-band nonlinear interactions and their suppression in multiwavelength-band WDM transmission systems. IEEE/OSA Journal on Lightwave Technology, 17:2249–2260, 1999.

[6] M. Born and E. Wolf. Principles of Optics: Electromagnetic Theory of Propagation, Diffraction and Interference of Light. Cambridge University Press, Cambridge, 1999.

[7] I. P. Kaminow and T. L. Koch, editors. Optical Fiber Telecommunications IIIA. Academic Press, San Diego, CA, 1997.

[8] R. W. Boyd. "Nonlinear Optics." 2nd ed. Academic Press, Inc., 2003

[9] E. A. J. Marcatili. "Bends in Optical Dielectric Guides." Bell. Syst. Tech. J., vol. 48, September1969. pp. 2103-2132.

[10] E. A. J. Marcatili. "Dielectric Rectangular Waveguide and Directional Coupler for Integrated Optics." Bell. Syst. Tech. J., vol. 48, September 1969. pp. 2071-2101.

[11] C. K. Madsen and J. H. Zhao. "A General Planar Waveguide Autoregressive Optical Filter." IEEE J. Lightwave Tech., vol. 14, no. 3, March 1996. pp. 437-447

[12] S. C. Hagness et al.. "FDTD Microcavity Simulations: Design and Experimental Realization of Waveguide-Coupled Single-Mode Ring and Whispering-Gallery-Mode Disk Resonators." IEEE J. Lightwave Tech., vol. 15, no. 11, November 1997. pp. 2145-2165

[13] D. Rafizadeh et al.. "Waveguide-coupled AlGaAs/GaAs microcavity ring and disk resonators with high finesse and 21.6 nm free spectral range." Opt. Lett., vol. 22, no. 16, August 1997. pp. 1244-1246

[14] B. E. Little et al.. "Ultra-Compact Si-SiO2 Microring resonator Optical Channel Dropping Filters." IEEE Photon. Techn. Lett., vol. 10, no. 4, April 1998. pp. 549-551

[15] D. J. W. Klunder et al., "Vertically and laterally waveguide-coupled cylindrical microresonators in Si3N4 on SiO2 technology." Appl. Phys. B 73., November 2001. pp. 603-608

[16] B. Vanderhaegen et al.. "High Q GaInAsP ring resonator filters." ECIO'99, Torino Italy, April 1999. pp. 381-384

[17] M. K. Chin et al.. "GaAs Microcavity Channel-Dropping Filter based on a Race-Track Resonator." IEEE Photon. Techn. Lett., vol. 11, no. 12, December 1999. pp. 1620-1622

[18] C. K. Madsen and J. H. Zhao, "Optical Filter Design and Analysis: A Signal Processing Approach." New York: Wiley, 1999

[19] J. E. Heebner and R.W. Boyd. "Enhanced all-optical switching by use of a nonlinear fiber ring resonator." Opt. Lett., vol. 24, no. 12, 1999. pp. 847–849

[20] Y. Su, F. Liu, and Q. Li, "System performance of slow-light buffering, and storage in silicon nano-waveguide", Proc. SPIE 6783, (2007)67832P.

[21] P.P. Yupapin, P. Saeung and C. Li, "Characteristics of complementary ring-resonator add/drop filters modeling by using graphical approach", Opt. Commun., 272(2007)81-86.

[22] P.P. Yupapin and W. Suwancharoen, "Chaotic signal generation and cancellation using a microring resonator incorporating an optical add/drop multiplexer", Opt. Commun., 280(2)(2007)343-350.2-364.

[23] M. Fujii, J. Leuthold and W. Freude, "Dispersion relation and loss of subwavelength confined mode of metal-dielectric-gap optical waveguides", IEEE Photon. Technol. Lett., 21(6)(2009)362-364.

[24] S. Mithata, N. Pornsuwancharoen and P.P. Yupapin, "A Simultaneous short wave and millimeter wave generation using a soliton pulse within a nano-waveguide", IEEE Photon. Technol. Lett., 21(13)(2009)932-934.

[25] Dominik G. Rabus. "Realization of Optical Filters using Ring Resonators with integrated Semiconductor Optical Amplifiers in GaInAsP / InP". Berlin,2002.

[26] R. W. Boyd: Nonlinear Optics, 2nd edn. (Academic, San Diego 2003)

[27] S. I. Wawilov, W. L. Lewschin: Die Beziehungen zwischen Fluoreszenz und Phosphoreszenz in festen und flüsssigen Medien, Z. Phys. **35**, 920–936 (1926)

[28] S. I. Vavilov: Microstructure of Light (USSR Acad. Sci., Moscow 1950)

[29] P. A. Franken, A. E. Hill, C. W. Peters, G. Weinrich: Generation of optical harmonics, Phys. Rev. Lett. **7**, 118 (1961)

[30] R. Terhune P. Maker, C. Savage: Observation of saturation effects in optical harmonic generation, Phys. Rev. Lett. **2**, 54 (1963)

[31] A. I. Kovrigin, A. S. Piskarskas, R. V. Khokhlov: On the generation of UV radiation by cascaded frequency conversion, Pis'ma Zh. Eksp. Teor. Fiz. **2**, 223 (1965)

[32] N. Bloembergen: Nonlinear Optics (Benjamin, New York 1964)

[33] S. A. Akhmanov, R. V. Khokhlov: Problems of Nonlinear Optics (VINITI, Moscow 1964) Engl. transl. New York, Gordon & Breach, 1972.

[34] Y. R. Shen: The Principles of Nonlinear Optics (Wiley, New York 1984)

[35] D. Cotter, P. N. Butcher: The Elements of Nonlinear Optics (Cambridge University Press, Cambridge 1990)

[36] J. F. Reintjes: Nonlinear Optical Parametric Processes in Liquids and Gases (Academic, Orlando 1984)

[37] Th. G. Brown, K. Creath, H. Kogelnik, M. A. Kriss, J. Schmit, M. J. Weber: The Optics Encyclopedia, ed. by Th. G. Brown, K. Creath, H. Kogelnik, M. A. Kriss, J. Schmit, M. J. Weber (Wiley-VCH, Weinheim 2004) Chap. Nonlinear Optics, p. 1617

BIOGRAPHY

Name: Mr. Chaiwat Sirawattananon

Date of Birth: February 8th , 1987

Address: 154 Moo 2 Naphralan Chalermphrakiat Saraburi 18240

Education: 2008 Bachelor's Degree in Computer Engineering, Bangkok University

Experience: Programmer

Skilled Works: Programming development

Database Management

Mobile Application